DECARBONIZATION OF THE CARGO SHIPPING FLEET

J. S. CHALFANT | L. BONFIGLIO | C. CHRYSSOSTOMIDIS
SEA GRANT DESIGN LABORATORY | MASSACHUSETTS INSTITUTE OF TECHNOLOGY

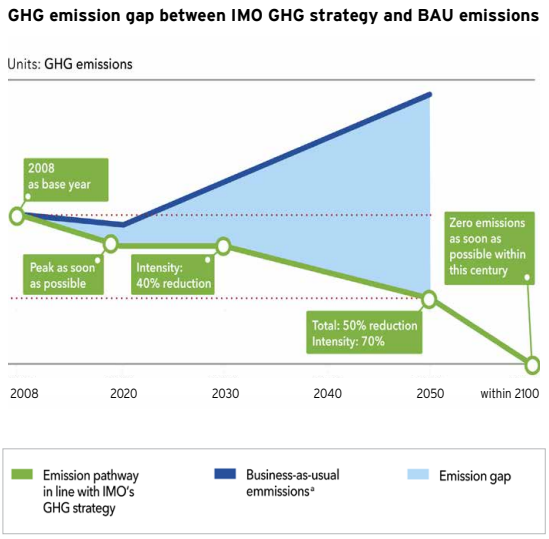

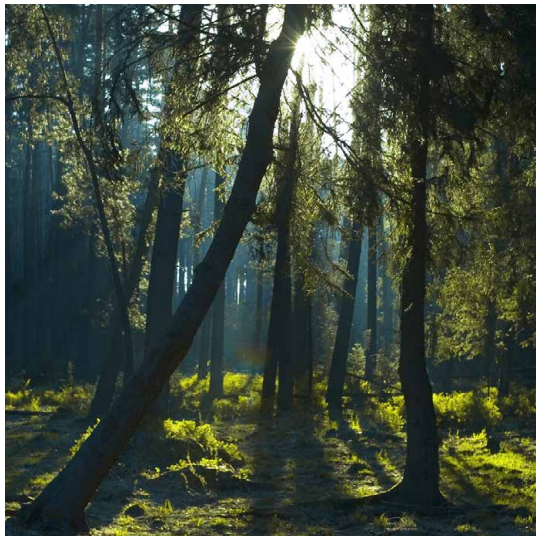

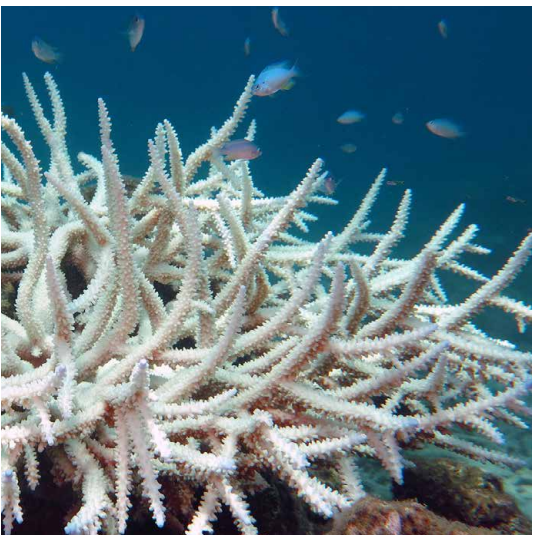

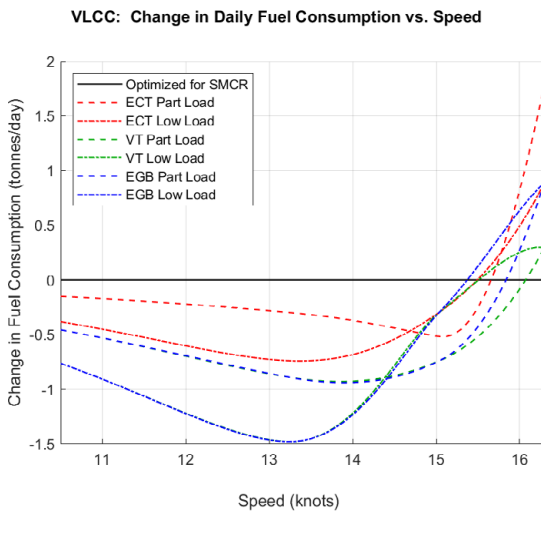

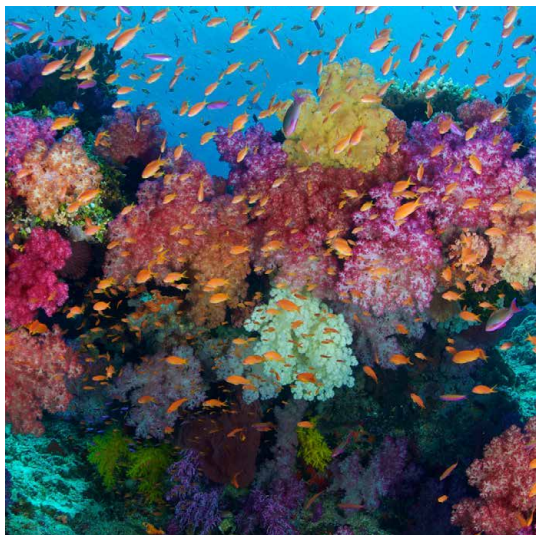

Cover art by Lily Keyes.

The front cover symbolizes the ravages of climate change, modified by improvements in greenhouse gas emissions, leading to recovery. The back cover illustrates the range of applicability of the code described in this report, including ship types, ballast conditions, and decarbonization methods and technologies.

Decarbonization of the Cargo Shipping Fleet

MIT Sea Grant Report Number 2019-R/RCM-64-LEV

J. S. Chalfant, L. Bonfiglio, C. Chryssostomidis
Sea Grant Design Laboratory
Massachusetts Institute of Technology
Cambridge, Massachusetts 02139
Email: chalfant@mit.edu

September 23, 2021

Executive Summary

In an effort to combat climate change, the International Maritime Organization (IMO) has set ambitious goals for the reduction of greenhouse gas emissions from ships, with a target of at least a 50% reduction of total annual greenhouse gas (GHG) emissions, including carbon, from 2008 levels by 2050, with a further goal of zero GHG emissions within this century [22]. Numerous interim goals guide the cargo fleet toward the 50% by 2050 target. It will take the combination of a large variety of actions and technology advancements to achieve these goals. Long-term possibilities such as the development and shipboard implementation of new fuels, renewable energy, and energy storage will have a huge impact on shipboard CO2 production, but there is great uncertainty about which of these technologies will become the best option for both the earth and the shipping companies. Numerous actions can be taken immediately to reduce the carbon production and extend the useful life of currently existing ships within the new GHG requirements, allowing ship owners time to assess new technologies before committing to new-construction vessels that incorporate them.

This report describes a methodology and computer code that provide a rapid assessment of the impact of various fuel-saving technologies on a cargo ship's fuel consumption, thus providing the ship owner fundamental data indicating which technologies and practices warrant further, more detailed investigation. These fuel-saving technologies and practices include slow steaming, engine modifications, bulbous bow removal, propeller optimization, and the installation of energy saving devices that modify flow through the propeller.

The assessment of a ship's performance uses a small amount of data readily accessible to the ship owner; it is assumed that the data available for the candidate vessel is insufficiently detailed to accomplish a full computational fluid dynamics (CFD) analysis, so various standard estimation methodologies are employed as described herein. The minimum data required include ship type, length, beam, draft, displacement, design speed, number of propellers, engine layout data, and indication of the presence of a bulbous bow or energy-saving device. The accuracy of resistance estimates can be improved by increasing the amount of data provided to the program including information such as bulbous bow dimensions, longitudinal center of buoyancy, hull shape coefficients, surface areas, and propeller details. If these additional data are not provided, the program estimates input values.

Results are provided in terms of fuel usage and savings for each potential modification and for combinations of modifications, showing tonnes/day of fuel over a range of speeds. Estimates for both fully-laden and ballast condition are provided.

The code has been applied to a wide variety of ship types including supertankers, product tankers, bulk carriers and container ships of various sizes, and the results were compared to actual measured data for the ships operating at sea, with very good correlation between the estimates and the measured data. The resistance estimates are better with greater fidelity of input data. They are most accurate within the friction-dominated speeds, showing differences from measured data in the range of three percent. Accuracy of results can drop somewhat at high, wave-dominated speeds, especially for ships with bulbous bows.

The code is written in Matlab and is available online at https://seagrant.mit.edu/decarbonization.

The attached report describes the underlying methodology, provides an overview and user's guide for the code, presents several examples, and makes some concluding remarks and suggestions for future work.

This material is based upon research funded by the Hightide Foundation in collaboration with Marsoft Inc.

CONTENTS

Decarbonization of the Cargo Shipping Fleet

I. Background

According to the National Oceanic and Atmospheric Administration, the amount of carbon dioxide in the atmosphere has increased by 1.78 ppm per year on average since 1980, and the increase is accelerating. Through the 1980s and 1990s, the increase was around 1.5-1.6 ppm per year, but the growth rate has averaged 2.4 ppm per year since 2010 [24].

Rising levels of carbon dioxide in the atmosphere adversely impact the environment in many ways. For example, increased levels of carbon dioxide dissolving in sea water increase the acidity of the oceans; as pH levels drop, organisms like oysters and corals have trouble maintaining their hard shells and skeletons made from calcium carbonate. If pH levels get too low, the calcium carbonate structures begin dissolving [19]. Another example can be found in the NOAA Arctic Report Card which each year shows an Arctic that is becoming warmer, less frozen and more fragile; the 2020 report includes data on high land-surface air temperatures, low snow extent, low minimum sea-ice extent, and extreme wildfires [25].

Shipping is the most carbon-efficient method of transporting cargo per tonne-km of cargo moved; a very large crude carrier (VLCC) ship emits 3 grams of carbon per tonne-km of cargo, compared to 80 for a 40-tonne truck and 435 for a 747 aircraft [4]. However, the efficiency of cargo shipping is juxtaposed against the sheer quantity of goods transported by ship over vast distances; per the UN Review of Marine Transport [21], approximately 80% of world trade by volume, or 70% by value, is carried by ship. This results in cargo shipping contributing between 2 and 3% of total worldwide carbon emissions per year.

In an effort to combat climate change, the International Maritime Organization (IMO) has set ambitious goals for the reduction of greenhouse gas emissions from ships, with a target of at least a 50% reduction of total annual greenhouse gas (GHG) emissions, including carbon, from 2008 levels, by 2050 [22]. Zero GHG emissions are desired sometime within this century. Numerous interim goals step the cargo fleet toward the 50% by 2050 target.

Combining a large variety of actions and technology advancements will be required to achieve these goals. Long-term possibilities such as the development and shipboard implementation of new fuels, renewable energy, and energy storage will have a huge impact on shipboard CO2 production, but there is great uncertainty about which of these technologies will become the best option for both the earth and the shipping companies.

While the research and development required to bring these new technologies to fruition is being accomplished, numerous actions can be taken immediately to reduce the carbon production and extend the useful life of currently existing ships within the new GHG requirements, thus allowing ship owners time to assess new technologies before committing to new-construction vessels that incorporate them.

II. Introduction

We have constructed an easy-to-use computer code that provides ship owners fundamental data indicating which technologies and practices are likely to have a significant impact on the owner's fleet by providing an assessment of the impact of various fuel-saving technologies on a specific cargo ship's fuel consumption. These fuel-saving technologies and practices include slow steaming, engine modifications, bulbous bow removal, propeller optimization, and energy-saving devices that modify the hull. For each modification or combination of modifications, the code provides quantified impact in terms of specific fuel consumption and tons per day for a given loading condition of a given ship.

The computer code created through this project accomplishes a rapid assessment of a ship's performance using a small amount of data. The code is designed to be easy to use, depending on ship data that is readily available to the ship owner.

The code calculates the ship resistance over a range of speeds, estimates propeller performance, and predicts engine performance, all at design draft. If ballast draft information is provided, similar calculations are accomplished at ballast condition as well. The code also estimates ship performance with the bulbous bow removed, with an energy saving device installed, with various engine modifications implemented, or with a modified propeller designed for a different design speed, and with combinations of these modifications. The primary metric for comparison is fuel consumption;

This document is arranged as follows. Section III provides an overview of the code structure and input data. Sections IV through VIII provide the theoretical background supporting hull, propeller and engine calculations. Section IX describes the methodology for assessing the impact of ship modifications on fuel consumption. Section X describes the calculations and estimates required to round out the data set. The code is used to analyze various ship types and the results are compared to actual ship performance; these examples are provided in Section XI. A user's manual is provided in Section XII. Additional discussion of bulbous bows is provided in the Appendix, followed by a glossary of terms, symbols and abbreviations. Conclusions and recommendations for future work are included in Section XIII.

III. Code Overview

Following is an overview of the program structure. Theoretical underpinnings of each segment along with a user's guide can be found in the subsequent sections. The original concept of the code is based on work by Bonfiglio [3].

A. Data Input

Input data are provided by the user in an Excel file. The minimum data required include ship type, length, beam, draft, displacement, design speed, number of propellers, engine layout data, and indication of the presence of a bulbous bow or energy-saving device. The accuracy of resistance estimates can be improved by increasing the amount of data provided to the program including information such as bulbous bow dimensions, longitudinal center of buoyancy, hull shape coefficients, surface areas, and propeller details. If these additional data are not provided, the program estimates input values.

Since full hullform and propeller models of sufficient detail to accomplish a full computational fluid dynamics (CFD) analysis of a hull are not typically available, we use instead various standard estimation methodologies for ship and propeller performance.

Incorporated into the program is a library of engines, including a wide range of MAN B&W and Wärtsilä marine diesel engines plus a few from other manufacturers. The library is stored in an Excel spreadsheet, to which the user may add new engines if desired.

During the data input period, the program reads and parses the input data, estimates missing data as appropriate, and sets constants.

B. As-Built Ship Calculations

For each ship in the input database, the following calculations are conducted:

1) Calculations at Design Draft:

a) Ship Resistance: Ship resistance is calculated at design draft using the Holtrop & Mennen procedure for tankers and bulkers or the Hollenbach procedure for container ships, producing curves of resistance and effective power over a range of speeds. Resistance estimates include frictional resistance, form factor, appendage resistance, wave resistance, bulbous bow impact, air resistance, and correlation allowance. Details are provided in Section IV and Section V.

b) Propeller Performance: Propeller performance is calculated using the Wageningen B-Series propeller regression formulas and the input data. If expanded area ratio (AE/AO) or pitch to diameter ratio (P/D) are not provided by the user, then the program designs a propeller that produces the lowest fuel oil consumption at design speed when coupled with the given engine, while limiting cavitation. Once AE/AO and P/D are set, the program calculates propeller efficiency, estimates hull efficiency and relative rotative efficiency, and uses the input shaft efficiency to calculate delivered and brake power over a range of speeds.

c) Engine Performance: The engine design operating point, termed specified maximum continuous rating (SMCR), is calculated using the brake power and rotation rate of the propeller at the design speed. Fuel oil consumption is calculated over the full range of speeds supported by the engine, assuming tuning at the SMCR point.

2) Calculations at Ballast Draft: If ballast draft information is provided, then the same ship hull/propeller/engine combination used in the design draft calculations is analyzed at ballast draft as follows:

a) Ship Resistance: Ship resistance is calculated at ballast draft, producing curves of resistance and effective power over a range of speeds at the appropriate draft.

b) Propeller Performance: The propeller curves determined at design draft are used to calculate propeller performance at ballast draft, providing estimates of delivered and brake power over a range of speeds.

c) Engine Performance: Using the SMCR point calculated at design draft, fuel oil consumption is calculated at ballast draft over the full range of speeds supported by the engine.

C. Performance Improvements

The following performance improvements can be calculated individually or in combinations. It is possible to combine any of these major modifications with any other, with the exception that only one engine modification can be selected at a time. Note that the impacts of combinations of improvements are not linear, so to calculate the overall impact, one must accomplish the analysis with multiple improvements selected, rather than summing the results of various individual improvements.

1) Engine Modifications: Estimates of fuel oil consumption for a variety of engine modifications appropriate to the installed engine are provided over the range of speeds available.

2) Propeller Optimization: The propeller may be redesigned for a slower design speed by removing the AE/AO and P/D from the input data and designating a new design speed and maximum speed for cavitation purposes.

3) Bulbous Bow Removal: If a bulbous bow is present, estimates for the impact of removing the bulbous bow are provided by reducing hull wetted surface area by the surface area of the bulb, and eliminating the bulbous bow impact in the resistance calculation.

4) Energy Saving Device Addition: The impact of adding an energy saving device can be estimated by changing the input flag to "yes."

D. Output Data

Output from the program is provided in numerical tables and in graphical format. Resistance data, propeller data, and fuel usage are provided along with tabulation of input and calculated values for all variables. Examples are provided in Section XI.

IV. Resistance Calculation: Holtrop & Mennen

Ship resistance for tankers and bulkers is estimated from basic hullform characteristics using the method developed by Holtrop and Mennen [9]–[12]. This method predicts full-scale ship resistance through a regression analysis of many towing-tank resistance model tests of various hullforms. While a specific range of applicability is not explicitly defined, Birk [1] estimates that the method is applicable to ships with a prismatic coefficient between 0.55 and 0.85, and a length to beam ratio between 3.9 and 9.5. The methodology estimates wave resistance, frictional resistance modified by a form factor, air resistance, a correction factor for roughness and ship form,

and the resistance impacts of appendages and bulbous bow as applicable; these are combined to predict ship resistance in calm water with no wind, referred to herein as ship resistance at trial condition, or R_{TC}. Figure 1 shows the calculated resistance data for an example ship.

In this section, we follow the description of Holtrop & Mennen's method as described in Birk [1], with some modification where noted due to incorporation of subsequent research.

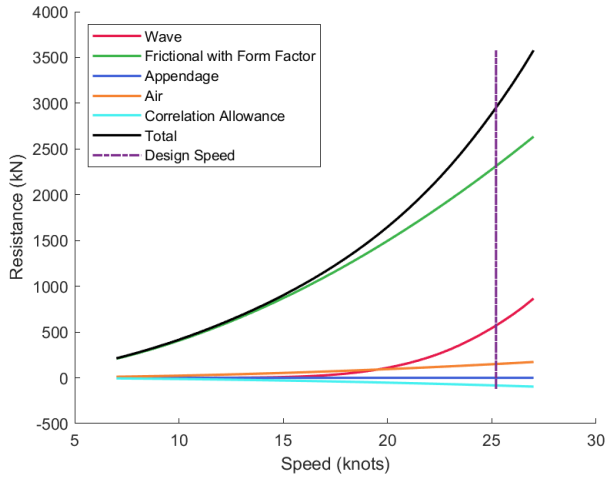

Fig. 1: Resistance calculated using Holtrop & Mennen procedure.

A. Wave Resistance

Holtrop & Mennen calculate wave resistance as a function of Froude number, Fr, in three regions such that

$$R_w = \begin{cases} R_{Wa}(Fr) & \text{when } Fr \leq 0.4 \\ R_{Wmid}(Fr) & \text{when } 0.4 < Fr \leq 0.55 \\ R_{Wb}(Fr) & \text{when } Fr > 0.55 \end{cases}$$

using

$$R_{Wa}(Fr) = \rho g \nabla c_{1a} c_2 c_5 e^{m_{1a} Fr^d + m_4 cos(\lambda Fr^{-2})}, \quad (1)$$

$$R_{Wb}(Fr) = \rho g \nabla c_{1b} c_2 c_5 e^{m_{1b} Fr^d + m_4 cos(\lambda Fr^{-2})}, \quad (2)$$

and

$$R_{Wmid} = R_{Wa}(0.4) + \frac{20Fr - 8}{3}\left[R_{Wb}(0.55) - R_{Wa}(0.4)\right]$$

where $R_{Wa}(0.4)$ indicates R_{Wa} evaluated at $Fr = 0.4$ and $R_{Wb}(0.55)$ indicates R_{Wb} evaluated at $Fr = 0.55$. The coefficients in these equations can be found in Table I.

B. Bulbous Bow Impact

Holtrop & Mennen account for the impact of the bulbous bow by applying a correction, c_2, to the wave resistance calculated using (1) and (2), thus reducing wave resistance when a bulbous bow is present. They suggest

$$c_2 = e^{-1.89\sqrt{c_3}}$$

where

$$c_3 = \frac{0.56 A_{bt}^{1.5}}{BT(0.31\sqrt{A_{bt}} + T_f - h_b)}, \quad (3)$$

A_{bt} is the transverse cross-sectional area of the bulb at the forward perpendicular, h_b is the height of the centroid of that area above baseline, and T_f is the draft at the forward perpendicular. This equation applies a reduction in wave resistance due to the bulbous bow; the reduction is a constant percentage of the wave resistance.

The frictional resistance impact of the bulb is inherently included in the frictional resistance calculation of Section IV-C since the ship wetted surface area includes the surface area of the bulb.

Note that the only characteristics of the bulb that are used in this calculation pertain to the area and centroid of the transverse cross-section of the bulb at the forward perpendicular; this is a small set of data to capture an extremely widely varying set of possible shapes and impacts of a bulbous bow, and is thus a very rough approximation of the impact of the bulb on the performance of the ship. See Appendix A for further discussion of the impact of a bulbous bow on ship performance.

C. Frictional Resistance

The frictional resistance, R_f, is calculated as

$$R_f = \frac{1}{2}\rho V^2 C_f A_{ws}$$

where ρ is the density of seawater, V is the ship speed, A_{ws} is the wetted surface area of the bare hull, and C_f is the non-dimensional coefficient of friction calculated using the ITTC-57 formula,

$$C_f = \frac{0.075}{(log_{10}(Re) - 2)^2}. \quad (4)$$

The frictional resistance coefficient is a function of Reynold's number, Re, a non-dimensional number indicating the turbulent nature of the flow. Re is the ratio of the inertial forces to the viscous forces.

$$Re = \frac{V L_{wl}}{\nu}$$

where V is the speed of the ship, L_{wl} is the length of waterline and ν is the kinematic viscosity of seawater, 1.1945×10^{-6} m^2/sec.

The frictional resistance calculated above is the resistance of a flat plate with wetted surface area A_{ws}. This frictional resistance is modified by a form factor, $(1+k)$, which accounts

TABLE I: Coefficients for wave resistance equations

$$
\begin{aligned}
c_{1a} &= 2223105 c_7^{3.78613} \Big(\frac{T}{B}\Big)^{1.07961} (90 - i_e)^{-1.37565} \\
c_{1b} &= 6919.3 C_x^{-1.3346} \Big(\frac{\nabla}{{L_{wl}}^3}\Big)^{2.00977} \Big(\frac{L_{wl}}{B} - 2\Big)^{1.40692} \\
c_5 &= 1 - \frac{0.8 A_x}{BTC_x} \\
c_7 &= \begin{cases} 0.229577 \Big(\frac{B}{L_{wl}}\Big)^{(1/3)} & \text{when } \Big(\frac{B}{L_{wl}}\Big) \le 0.11 \\ \Big(\frac{B}{L_{wl}}\Big) & \text{when } 0.11 < \Big(\frac{B}{L_{wl}}\Big) \le 0.25 \\ 0.5 - 0.0625 \Big(\frac{L_{wl}}{B}\Big) & \text{when } \Big(\frac{B}{L_{wl}}\Big) > 0.25 \end{cases} \\
c_{15} &= \begin{cases} -1.69385 & \text{when } (L_{wl}^3/\nabla) \le 512 \\ -1.69385 + ((L_{wl}{}^3/\nabla) - 8.0)/2.36 & \text{when } 512 < (L_{wl}^3/\nabla) \le 1726.91 \\ 0 & \text{when } (L_{wl}^3/\nabla) > 1726.91 \end{cases} \\
c_{16} &= \begin{cases} 8.07981 C_p - 13.8673 C_p^2 + 6.984388 C_p^3 & \text{when } C_p \le 0.8 \\ 1.73014 - 0.7067 C_p & \text{when } C_p > 0.8 \end{cases} \\
d &= -0.9 \\
i_e &= 1 + 89 e^a \\
a &= -\Big[\Big(\frac{L_{wl}}{B}\Big)^{0.80856} \Big(1 - C_{wp}\Big)^{0.30484} \Big(\frac{L_r}{B}\Big)^{0.34574} \Big(1 - C_p - 0.0225 lcb\Big)^{0.6367} \Big(\frac{100\nabla}{{L_{wl}}^3}\Big)^{0.16302}\Big] \\
m_{1a} &= 0.0140407 \frac{L_{wl}}{T} - 1.75254 \frac{\nabla^{(1/3)}}{L_{wl}} - 4.79323 \frac{B}{L_{wl}} - c_{16} \\
m_{1b} &= -7.2035 \Big(\frac{B}{L_{wl}}\Big)^{0.326869} \Big(\frac{T}{B}\Big)^{0.605375} \\
m4 &= 0.4 c_{15} e^{-0.034 Fr^{-3.29}} \\
\lambda &= \begin{cases} 1.446 C_p - 0.03 L_{wl}/B & \text{when } L_{wl}/B \le 12 \\ 1.446 C_p - 0.36 & \text{when } L_{wl}/B > 12 \end{cases} \\
L_r &= L_{wl}\Big(1 - C_p + \frac{0.06 C_p lcb}{4C_p - 1}\Big)
\end{aligned}
$$

for differences between the ship's form and a flat plate.

$$
\begin{aligned}
(1+k) &= 0.93 + \\
&\Big[0.487118(1 + 0.011 C_{stern})\Big(\frac{B}{L_{wl}}\Big)^{1.06806} \\
&\cdot \Big(\frac{T}{L_{wl}}\Big)^{0.46106} \Big(\frac{L_{wl}}{L_r}\Big)^{0.121563} \\
&\cdot \Big(\frac{{L_{wl}}^3}{\nabla}\Big)^{0.36486} (1 - C_p)^{-0.604247}\Big]
\end{aligned}
$$

where B is the beam at waterline, T is mean draft, L_r is the length of run defined in Table I, ∇ is the volumetric displacement, C_p is the prismatic coefficient, and the stern shape parameter, C_{stern}, is shown in Table II for various aft body shapes.

TABLE II: Stern shape parameters

Stern Shape	C_{stern}
pram with gondola	-25
V-shaped sections	-10
normal sections	0
U-shaped sections	+10

D. Appendage Resistance

Each type of appendage has an associated appendage resistance factor as shown in Table III, modified slightly from [1].

TABLE III: Form factors $(1 + k_2)$ for various types of appendages

rudder behind skeg	0.35
rudder behind stern	0.5
twin screw rudder (slender)	1.5
twin screw rudder (thick)	2.5
shaft brackets	3.0
skeg	0.75
strut bossing	2.5
hull bossing	1.0
exposed shaft ($\angle$ with buttocks $\sim 10^\circ$)	1.0
exposed shaft ($\angle$ with buttocks $\sim 20^\circ$)	1.0
stabilizer fins	1.8
dome	1.7
bilge keels	0.4

The total appendage resistance, R_{app}, is

$$R_{app} = \frac{1}{2}\rho V^2 C_f \sum_i (S_{app})_i (1 + k_2)_i$$

where C_f is the frictional resistance coefficient calculated in (4), and S_{app_i} is the surface area of the i_{th} appendage with corresponding appendage resistance factor $(1 + k_2)_i$.

E. Air Resistance

Total air resistance, R_{aa} is calculated as

$$R_{aa} = \frac{1}{2}\rho_a V^2 C_{aa} A_{exp}$$

where ρ_a is the density of air; A_{exp} is the area of the ship exposed to wind, which is area of the ship above the waterline including deckhouse and any loaded cargo, facing forward; and C_{aa} is assumed to be 0.8, an average value for typical ship structures.

F. Correlation Allowance

A correlation allowance accounts for differences between model and full scale results for effects such as roughness allowance and the partial dynamic similarity of the model test. While correlation allowances have historically been assigned a constant value of 0.0004, it has been found more recently that the correlation allowance should be varied with size of the vessel. A variety of correlation allowances are proposed by different authors; we use an estimate from Kristensen and Lützen [14]

$$C_a = \frac{0.5(log_{10}\Delta) - 0.1(log_{10}\Delta)^2}{1000}$$

where Δ is the ship displacement in metric tonnes. A lower limit of -0.0001 is placed on C_a. The correlation allowance resistance adjustment, R_a, is

$$R_a = \frac{1}{2}\rho V^2 C_a \Big[A_{ws} + \sum_i S_{app_i}\Big].$$

Note that the correlation allowance can be negative, in which case it reduces the total calculated resistance.

G. Total Resistance

Total resistance at trial condition, R_{TC}, is the total resistance in calm, deep water with no wind, and is merely the sum of the resistance components calculated above:

$$R_{TC} = R_f(1+k) + R_{app} + R_w + R_a + R_{aa}. \quad (5)$$

Holtrop and Mennen's original research included values for transom resistance and change in pressure due to the bulbous bow, but subsequent research indicates that both values should be omitted.

V. Resistance Calculation: Hollenbach

Ship resistance for container ships is estimated using the method developed by Hollenbach, which is a regression analysis of tow tank data taken in Vienna, Austria. Hollenbach provides a mean estimate of resistance along with an upper and lower bound. For our purposes, we use only the mean value. Hollenbach's method is applicable to displacement vessels with a length-to-beam ratio between 4.7 and 7.11, a beam-to-draft ratio from 1.99 to 4.00, and a block coefficient below 0.83. It provides separate analyses for design draft and ballast condition. We follow the description of the method provided by [1]. Figure 2 shows the calculated resistance data for an example ship.

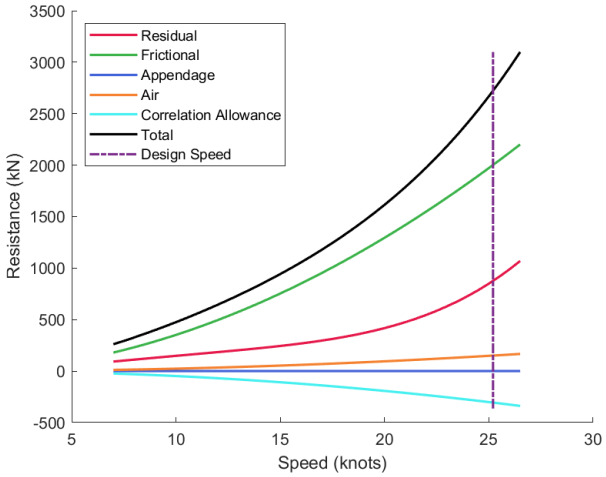

Fig. 2: Resistance calculated using Hollenbach procedure.

A. Calculation Length

A calculation length, L_c, is found using

$$L_c = L_{os} \text{ if } L_{os} < L_{bp} \quad (6)$$

$$L_{bp} + \frac{2}{3}(L_{os} - L_{bp}) \text{ if } L_{bp} < L_{os} < 1.1L_{bp} \quad (7)$$

$$1.0667L_{bp} \text{ if } L_{os} > 1.1L_{bp} \quad (8)$$

where L_{os} is the length over wetted surface.

B. Residuary Resistance

Since the frictional resistance calculation does not include a form factor, the residuary resistance, R_r, includes the effects of both wave resistance and the viscous pressure resistance. The coefficient of residuary resistance, C_r, uses a basis of beam times draft instead of the usual wetted surface area:

$$C_r = \frac{10R_r}{\frac{1}{2}\rho V^2 BT}.$$

We begin by calculating a standard coefficient, C_{rstd},

$$\begin{aligned} C_{rstd} = {} & b_{11} + b_{12}Fr + b_{13}Fr^2 \\ & +(b_{21} + b_{22}Fr + b_{23}Fr^2)C_b \\ & +(b_{31} + b_{32}Fr + b_{33}Fr^2)C_b^2 \end{aligned}$$

Note that the Froude number, Fr, is calculated using the calculation length, L_c, and the block coefficient, C_b, is calculated using the waterline length, L_{wl}. Coefficient values can be found in Table IV.

The coefficient b_{11} is corrected for single-screw vessels at design draft whose block coefficient is less than 0.6 as follows:

$$b_{11} = -0.87674 \quad \text{if } C_b < 0.49$$

$$b_{11} = -0.57424 - 25(0.6 - C_b)^2 \quad \text{if } 0.49 \le C_b < 0.6$$

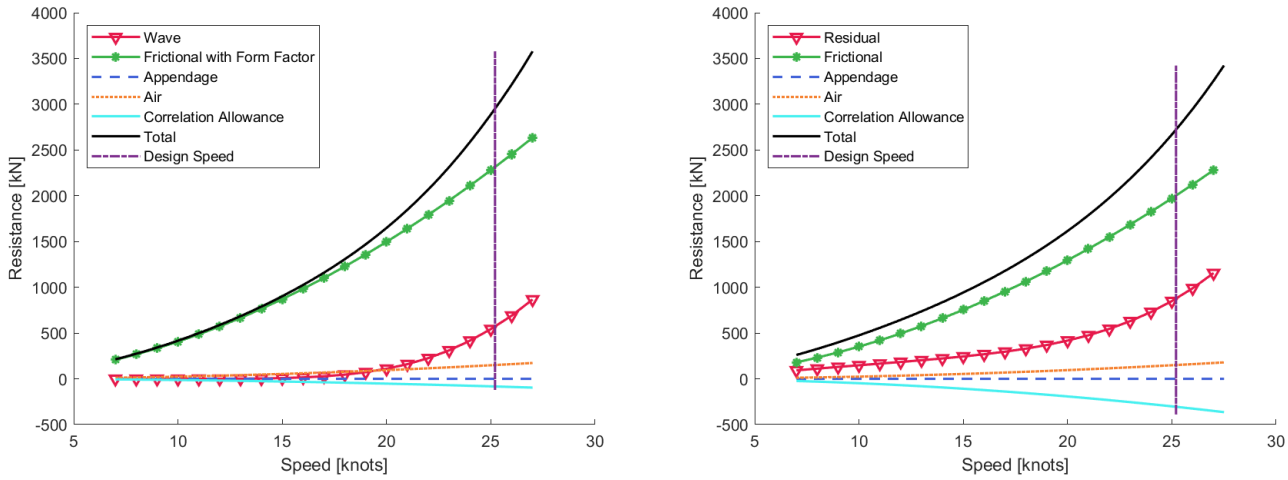

Fig. 3: Resistance calculated using Holtrop & Mennen procedure (left) and using Hollenbach procedure (right).

	single screw design draft	single screw ballast draft	twin screw design draft
b_{11}	-0.57424	-1.50162	-5.3475
b_{12}	13.3893	12.9678	55.6532
b_{13}	90.596	-36.7985	-114.905
b_{21}	4.6614	5.55536	19.2714
b_{22}	-39.721	-45.8815	-192.388
b_{23}	-351.483	121.82	388.33
b_{31}	-1.14215	-4.33571	-14.3571
b_{32}	-12.3296	36.0782	142.738
b_{33}	459.254	-85.3741	-254.762

TABLE IV: Coefficients for calculation of residuary resistance

	single screw design draft	single screw ballast draft	twin screw design draft
a_1	0.3382	0.7139	0.2748
a_2	-0.8086	-0.2558	-0.5747
a_3	-6.0258	-1.1606	-6.761
a_4	-3.5632	0.4534	-4.3834
a_5	9.4405	11.222	8.8158
a_6	0.0146	0.4562	-0.1418
a_7	0.0	0.0	-0.1258
a_8	0.0	0.0	0.0481
a_9	0.0	0.0	0.1699
a_{10}	0.0	0.0	0.0728
d_1	0.854	0.032	0.897
d_2	-1.228	0.803	-1.457
d_3	0.497	0.739	0.767
e_1	2.1701	1.9994	1.8319
e_2	-0.1602	-0.1446	-0.1237

TABLE V: Coefficient values for additional factors to residuary resistance

The standard residuary resistance is affected by a multitude of parameters, described below. Coefficients for the equations can be found in Table V.

For speeds above a critical Froude number Fr_c, the high Froude number factor, k_{Fr}, is

$$k_{Fr} = 1 \qquad \text{if } Fr < Fr_c$$
$$k_{Fr} = \left(\frac{Fr}{Fr_c}\right)^{c_1} \qquad \text{if } Fr > Fr_c$$

where

$$Fr_c = d_1 + d_2 C_b + d_3 C_b^2$$

and $c_1 = Fr/Fr_c$ for single and twin screw vessels at design draft, and $c_1 = 10C_b((Fr/Fr_c) - 1)$ for single screw vessels at ballast draft.

The length factor, k_L, is

$$k_L = e_1 (L_{bp})^{e_2}$$

in which L_{bp} must be entered in meters.

The beam-to-draft ratio factor, k_{bt}, is

$$k_{bt} = (1.99)^{a_1} \qquad \text{if } B/T \leq 1.99$$
$$k_{bt} = (B/T)^{a_1} \qquad \text{if } B/T > 1.99$$

The length-to-beam ratio factor, k_{lb}, is

$$k_{lb} = (L_{bp}/B)^{a_2} \qquad \text{if } L_{bp}/B \leq 7.11$$
$$k_{lb} = (7.11)^{a_2} \qquad \text{if } L_{bp}/B > 7.11$$

The wetted length factor, k_{ll}, is

$$k_{ll} = (L_{os}/L_{wl})^{a_3} \qquad \text{if } L_{os}/L_{wl} \leq 1.05$$
$$k_{ll} = (1.05)^{a_3} \qquad \text{if } L_{os}/L_{wl} > 1.05$$

The aft overhang ratio factor, k_{ao}, is

$$k_{ao} = (L_{wl}/L_{bp})^{a_4} \qquad \text{if } L_{wl}/L_{bp} \leq 1.06$$
$$k_{ao} = (1.06)^{a_4} \qquad \text{if } L_{wl}/L_{bp} > 1.06$$

The trim correction factor, k_{tr}, is

$$k_{tr} = \left[1 + \frac{T_a - T_f}{L_{bp}}\right]^{a_5}$$

The propeller correction factor, k_p, is

$$\begin{aligned} k_p &= (0.43)^{a_6} && \text{if } D/T_a < 0.43 \\ k_p &= (D/T_a)^{a_6} && \text{if } 0.43 \leq D/T_a < 0.84 \\ k_p &= (0.84)^{a_6} && \text{if } 0.84 \leq D/T_a \end{aligned}$$

The standard residuary resistance is then multiplied by several factors for additional influences such that

$$\begin{aligned} C_{rbt} =& C_{rstd} \cdot k_{Fr} \cdot k_L \cdot k_{bt} \cdot k_{lb} \cdot k_{ll} \cdot k_{ao} \cdot k_{tr} \cdot k_p \\ & \cdot N_{rudder}^{a_7} \cdot N_{brackets}^{a_8} \cdot N_{bossings}^{a_9} \cdot N_{thrusters}^{a_{10}}. \end{aligned}$$

where N_{rudder} is the number of rudders (1 or 2, for twin screw vessels), $N_{brackets}$ is the number of shaft brackets (0, 1 or 2, for twin screw vessels), $N_{bossings}$ is the number of shaft bossings (0, 1 or 2, for twin screw vessels), and $N_{thrusters}$ is the number of side thrusters (between 0 and 4).

Hollenbach's residuary resistance coefficient, C_{rbt}, is based on a reference surface of $BT/10$; this is converted to a wetted surface area basis such that the residuary resistance coefficient used herein, C_r, is

$$C_r = C_{rbt} \frac{BT}{10 A_{ws}}$$

and the residuary resistance, R_r, is

$$R_r = \frac{1}{2} C_r \rho V^2 A_{ws}.$$

C. Frictional Resistance

Hollenbach uses the ITTC 1957 model-ship correlation line, (4), with no form factor, using a Reynold's number based on L_c.

D. Appendage and Air Resistances

The appendage and air resistance values, R_{app} and R_{aa} respectively, are calculated using the equations provided by Holtrop & Mennen.

E. Correlation Allowance

The correlation allowance used by Hollenbach coincides with the Vienna Model Basin, such that

$$C_a = (0.35 - 0.002 L_{bp}) 10^{-3}$$

and the associated resistance, R_a is

$$R_a = \frac{1}{2} C_a \rho V^2 A_{ws}.$$

Although Hollenbach limits the correlation allowance to a minimum of zero, we extend this for larger ships to allow the correlation allowance to reach a minimum of -0.0001, consistent with the practice we use for Holtrop & Mennen.

F. Total Resistance

Total resistance is the sum of all individual resistances, such that

$$R_{TC} = R_f + R_r + R_{app} + R_a + R_{aa}.$$

VI. Propeller Calculation

Propeller performance characteristics are estimated using the Wageningen B-series propeller data as described in [15]. This regression analysis provides thrust coefficient (K_T), torque coefficient (K_Q), and open-water efficiency (η_o) as a function of advance ratio (J), based on the provided values of diameter (D), number of blades (Z), pitch/diameter ratio (P/D), and expanded area ratio (AE/AO). We address herein only fixed-pitch propellers with one propeller per shaft; counter-rotating propellers and controllable-pitch propellers are not addressed.

A. Resistance Input to Propeller Calculation

Ship resistance versus speed is calculated using the method described in Section IV or V above, producing "trial condition" resistance (R_{TC}), *i.e.* resistance in deep, calm water with no wind.

The "heavy running" resistance (R_{HR}), which includes the impact of wind and waves, is estimated by increasing the calm water resistance by a sea margin, sm, provided by the user

$$R_{HR} = R_{TC}(1 + sm). \tag{9}$$

The sea margin can vary depending on the type of ship and the planned operational area, but a typical value is 15%; this is the value assumed if the user does not input a value.

If the ship is not at even keel, then the thrust from the propeller is not directly forward. Therefore, the thrust is increased by a trim factor

$$F_{trim} = \sqrt{1 - \left(\frac{|T_a - T_f|}{L_{bp}} \right)^2} \tag{10}$$

where T_a is draft at the aft perpendicular, T_f is the draft at the forward perpendicular, and L_{bp} is the ship length between perpendiculars. For a twin-screw ship, we assume equal loading of the propellers, so the thrust for each propeller is one-half of the total thrust. Thus, the resistance value used in estimating propeller performance, R_T, is

$$R_T = \frac{R_{HR}}{F_{trim} N_p} \tag{11}$$

where N_p is the number of propellers.

B. Propeller Curves

The non-dimensional advance ratio of the propeller is the ratio of the fluid speed over the propeller tip speed:

$$J = \frac{V_a}{nD} \tag{12}$$

where V_a is the water speed at the propeller, n is the rotation rate, and D is the propeller diameter. Since the propeller is located in the wake of the ship, the fluid speed seen by the propeller is most likely not equal to the speed of the ship. The wake fraction, w, accounts for this difference and is used to determine water speed relative to ship speed, V, such that

$$V_a = V(1 - w). \tag{13}$$

The defining curves for propeller performance in open water are the non-dimensional thrust coefficient, K_T,

$$K_T = \frac{T_o}{\rho n^2 D^4}$$

and the non-dimensional and torque coefficient, K_Q,

$$K_Q = \frac{Q_o}{\rho n^2 D^5}$$

where Q_o is open water torque. T_o is open water thrust, defined as

$$T_o = \frac{R_T}{(1-t)}$$

where t is the thrust deduction factor. A propeller operating in close proximity to a hull creates a low pressure region on the intake side near the hull, thus slightly increasing the resistance of the vessel. This effect is accounted for using the thrust deduction factor, t, which is a function of the shape of the hull and the size of the propeller.

The open water efficiency of the propeller is

$$\eta_o = \frac{JK_T}{2\pi K_Q}. \tag{14}$$

Propeller curves for a representative propeller are plotted versus J in Figure 4.

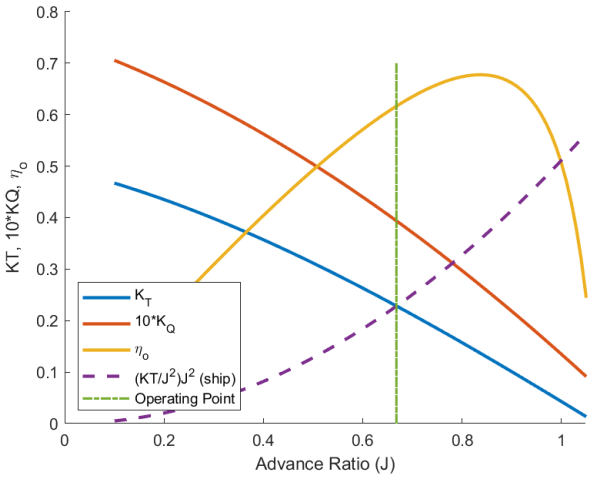

Fig. 4: Propeller curves. The propeller operating point at a given speed is determined by the intersection of the ship-specific K_T curve and the propeller-specific K_T curve.

We assume that the Wageningen B-Series propeller is indicative of the propeller used in the ship, and calculate the performance characteristics of the propeller using the regression formula coefficients as described in [15]. We have found this to be a good assumption in all cases for which we have propeller data.

The K_T and K_Q curves are estimated using

$$K_T = \sum C_{kt} Z^{zt} (AE/AO)^{at} (P/D)^{pt} J^{jt} \tag{15}$$

$$K_Q = \sum C_{kq} Z^{zq} (AE/AO)^{aq} (P/D)^{pq} J^{jq} \tag{16}$$

where Z is the number of blades, AE/AO is the expanded area ratio, P/D is the pitch to diameter ratio, and C_{kt}, C_{kq}, zt, at, pt, jt, zq, aq, pq and jq are coefficients and terms of the Wageningen B-screw Series found in [15].

If the number of blades is not provided by the user, we assume four. If the pitch to diameter ratio is not provided, we choose the P/D ratio that produces the best fuel oil consumption at design speed, using the methodology described in Section IX-B. If the expanded area ratio is not provided, we use the formulation proposed by Keller and reported in [1] in which

$$AE/AO = \frac{(1.3 + 0.3Z)T_o}{(p_o - p_v)D^2} + k \tag{17}$$

where Z is the number of blades, T_o is the thrust, $(p_o - p_v)$ is the pressure at the centerline of the propeller, and k is a constant that varies with the type of ship. We use $k = 0.2$ for single-screw vessels, $k = 0.1$ for high-speed twin-screw vessels (with design speeds greater than 20 knots), and $k = 0.0$ for slower twin-screw vessels. The Keller criteria selects an expanded area ratio that is likely to meet cavitation criteria. After calculating propeller performance, we estimate cavitation and adjust AE/AO if necessary; please see the discussion of cavitation in Section VI-D.

C. Propeller Operating Point

To remove the dependence of the propeller curves on propeller rotation rate, which is unknown at this point, we divide K_T by J^2

$$\frac{K_T}{J^2} = \frac{T_o}{\rho D^2 V_a^2} \tag{18}$$

where T_o and V_a are calculated as described above, and D is provided by the user or estimated.

At any given speed and sea state, the intersection of the curve defined by (18) multiplied by J^2 (for the particulars of the ship), and the propeller K_T curve defined by (15) (for the particulars of the propeller), determines the J value at which the propeller will operate when installed in the given ship at the given speed and sea state; an example is shown in Figure 4.

Once J is determined for a given operating point, the propeller rotation rate and open water propeller efficiency can be calculated at that speed and sea state using (12) and (14). We thus produce, for the trial condition and the heavy running condition, curves of delivered power versus ship speed, propeller rotation rate versus ship speed, and propeller efficiency versus ship speed. Examples are shown in Figure 5.

D. Cavitation

Cavitation occurs when the local pressure falls below the vapor pressure, causing bubbles to form and collapse, which

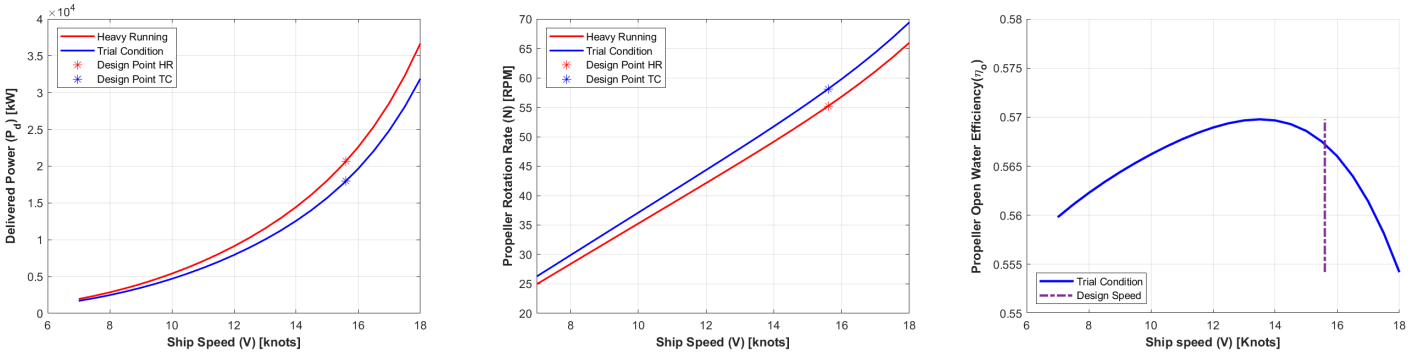

Fig. 5: Delivered power (left), propeller rotation rate (center) and propeller open-water efficiency (right) as functions of ship speed.

in turn cause noise, vibration, damage to the propeller, and a significant reduction in thrust provided by the propeller. While some small amount of cavitation is acceptable, the propeller must be designed to perform appropriately over the full range of desired speeds. Typically, risk of cavitation is reduced with increased blade area.

Burrill developed a criteria for predicting cavitation in 1943 and revised it in 1962-63. He presented likelihood of cavitation based on a cavitation number and thrust coefficient; the well-known Burrill diagram, shown in Figure 6 from [20], is used in the early stages of propeller design to avoid cavitation. The cavitation number, σ, is derived from Bernoulli and defined as [20]

$$\sigma = \frac{p_{atm} + \rho g h - p_v}{q_T}$$

where p_{atm} is atmospheric pressure at the surface, ρ is the density of sea water, g is the gravitational constant, h is the distance from the water surface to the centerline of the propeller, p_v is the vapor pressure of sea water, and

$$q_T = \frac{1}{2}\rho(V_R)^2$$

where V_R, the relative velocity of water with respect to the propeller at 0.7 radius, is

$$V_R = V(1-w)\sqrt{1+(0.7\pi/J)^2}$$

in which V is ship speed, w is wake fraction, and J is propeller advance ratio. The thrust coefficient, τ_c, is used to express the mean thrust loading on the blades [20];

$$\tau_c = \frac{Th}{q_T A_P}$$

where Th is the thrust and A_P is projected blade area. The projected blade area can be estimated from the expanded area, A_E, using

$$A_P = A_E(1.067 - 0.229\frac{P}{D}).$$

Burrill recommended a limit of 5% back cavitation for merchant ship propellers; however, numerous more recent studies

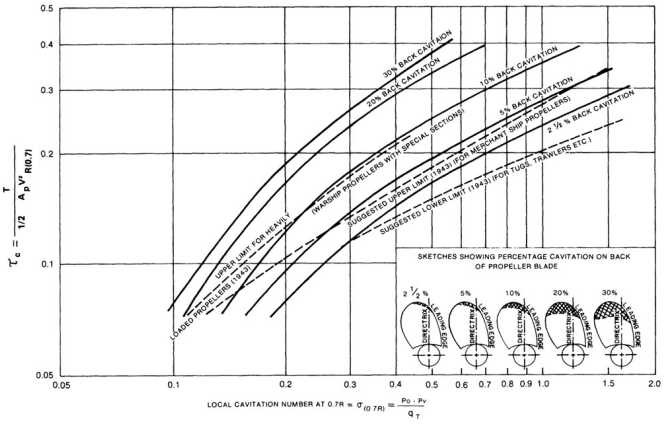

Fig. 6: Burrill diagram [20].

of cavitation indicate a higher back cavitation limit is more appropriate; see, for example, [2], [6]. The American Bureau of Shipping (ABS) guidance [20] states that modern merchant ship propellers are designed with airfoil blade sections, making the 10% back cavitation line more appropriate.

Due to these recommendations, we limit ship speed to the speed that corresponds with 10% back cavitation. If this limit falls below the design speed, we increase blade area until the cavitation criteria is met. Figure 7 shows the cavitation limit for a sample ship; the top diagram plots mean thrust loading versus cavitation limit and the bottom diagram plots mean thrust loading versus ship speed. In this example, the cavitation limit occurs at 15.5 knots, which is above the ship design speed of 15.3 knots. The user may input a maximum speed, different from the design speed, which the program will ensure is met without significant cavitation through appropriate selection of AE/AO.

E. Propulsion Power

Having determined the resistance of the ship and the performance of the propeller, we now determine the power required

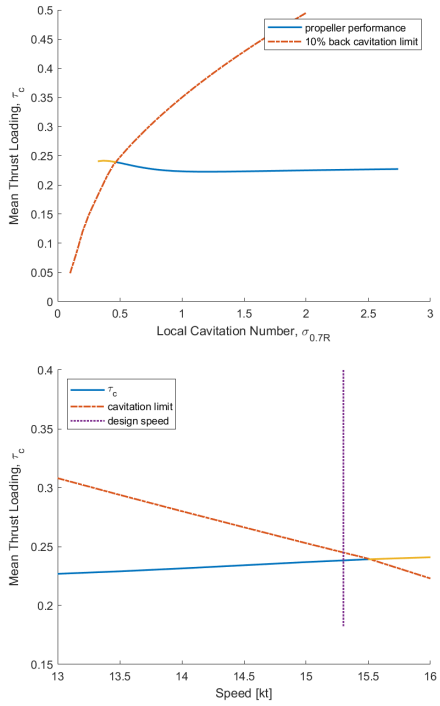

Fig. 7: Cavitation limit example; the cavitation limit of this vessel is 15.5 knots, which is above the design speed of 15.3 knots, as shown in the lower figure.

to propel the ship through the water.

Effective power, P_e, is the power required to overcome the resistance of the ship.

$$P_e = R_T V.$$

Delivered power, P_d, is the power that must be delivered to the propeller in place and incorporates the effects of propeller efficiency, hull efficiency, and relative rotative efficiency.

$$P_d = \frac{P_e}{\eta_o \eta_h \eta_r}$$

where hull efficiency, η_h, is

$$\eta_h = \frac{1-w}{1-t}.$$

Brake power, P_b, is the power that must be produced by the engine; it incorporates the shaft efficiency, η_s.

$$P_b = P_d/\eta_s$$

where η_s is a scalar value provided by the user. If not provided, we assume η_s = 0.99. The shaft efficiency accounts for losses along the shaft due to bearings and other frictional losses.

See Figure 8 for a representation of the various power values.

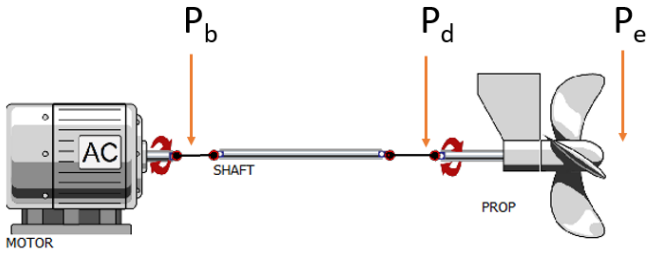

Fig. 8: Effective power (P_e), delivered power (P_d), and brake power (P_b).

VII. Engine Calculations

We assume that all power generated by the engine goes to propulsion and that no reduction gear is used; thus, the rotation rate of the engine is equal to the rotation rate of the propeller and the load on the engine is equal to the load on the propeller, increased by the relevant efficiencies.

Each diesel engine has a characteristic layout diagram defined by four points, $L1$, $L2$, $L3$ and $L4$; see Figure 9 for examples. The $L1$ point is the engine's nominal maximum continuous rating (MCR), which is the rated sustained maximum power produced by the engine at the rated sustained maximum rotation rate; these maximum power and rotation rate values can be exceeded by the engine, but only for a short period of time. The line from $L1$ to $L3$ on a log-log plot is a line of constant mean effective pressure (MEP) at the maximum rated MEP for the engine. Lines of constant MEP are parallel to the $L1 - L3$ line.

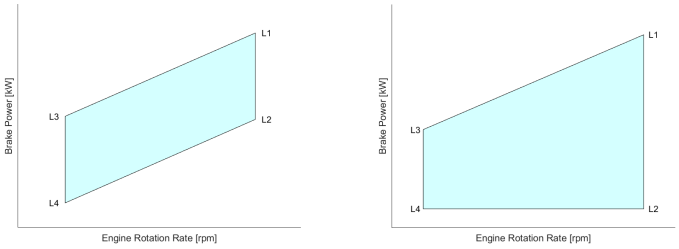

Fig. 9: Representative engine layout diagrams.

The ship operational design point is the power and rotation rate required to achieve design speed at a selected design sea state including an engine margin, em, and a propeller margin, pm; this operational design point is termed the specified maximum continuous rating (SMCR). We define brake power at SMCR as

$$Pb_{SMCR} = Pb_{hrDes}(1 + em)$$

where Pb_{hrDes} is the brake power for heavy running at design speed and em is the engine margin, typically 10%. The corresponding engine speed, N_{SMCR}, is the value of the

engine speed curve at the SMCR power, N_{hrDes}, decreased by a propeller margin, pm, typically 5%, such that

$$N_{SMCR} = N_{hrDes}(1 - pm).$$

The SMCR point, defined by the power, Pb_{SMCR}, and the rotation rate, N_{SMCR}, must fall within the engine layout diagram.

To clarify the difference between MCR and SMCR, the MCR is the maximum rated power and speed combination that can be produced by the engine; the SMCR is the maximum rated power and speed combination that can be produced by the engine *as installed in the ship* and includes such impacts as coupling with the propeller and tuning for the application.

The entire operating curve of the engine at all planned speeds and sea states must fall within an area defined by speed, power, mean effective pressure, and torque limits of the engine as installed. An example plot is shown in Figure 10; note that the trial condition and heavy running propeller curves (solid and dashed black lines) are within the designated limits of the engine as installed. Details for calculation of the limiting curves may be found in [16].

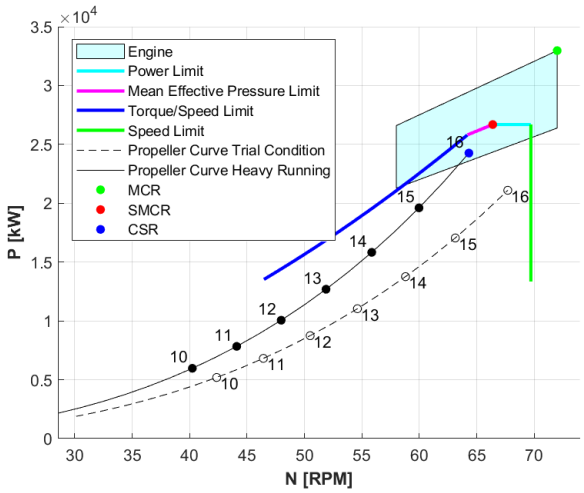

Fig. 10: Representative engine load diagram and operating limits for an engine installed in a ship. The numbers on the propeller curves correspond to ship speed in knots.

A. Engine Performance

Specific fuel oil consumption (SFOC) for an engine varies with mean effective pressure and engine load. We determine the SFOC at 100% engine load by calculating the MEP at SMCR as a percentage of maximum MEP, then using the change in SFOC with MEP to determine SFOC at SMCR. The change in SFOC with MEP is provided in the engine data input.

The SMCR data point is then used to determine SFOC as a function of engine load. Change in SFOC engine load is provided as an input in the engine data. If unavailable, generic values are used as an estimate; Figure 11 is an example.

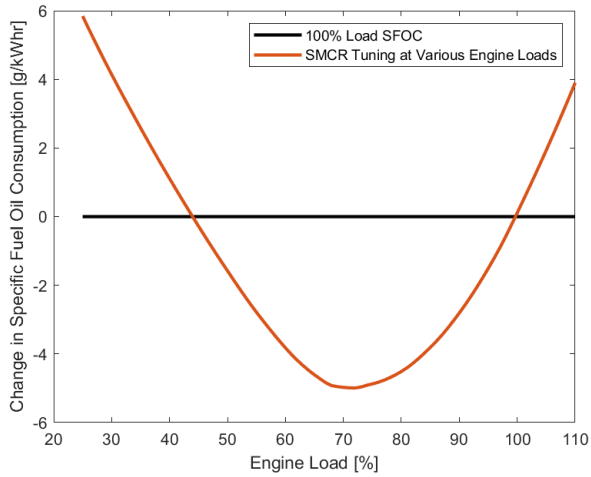

Fig. 11: Sample change in SFOC with engine load for a typical two-stroke low-speed diesel engine.

Combining the SFOC versus engine load data with the speed/power curve data determined in Section IV or V above allows us to determine fuel oil consumption (FOC) in tons per day as a function of speed for an engine tuned to the SMCR at high load.

$$FOC = SFOC \cdot P_b \tag{19}$$

The engine is typically tuned so that peak fuel efficiency occurs between 70 and 80% engine load; this point is termed the continuous service rating (CSR).

VIII. Limits on Ship Speed

The lower bound on ship speed for the resistance and propeller calculations is set to 7 knots, and the upper bound is set to 1 knot greater than design speed, rounded up to the nearest whole knot, or by the Froude number limit from the resistance calculation, whichever is lower. Fr is the Froude number, defined as

$$Fr = \frac{V}{\sqrt{gL}}$$

where V is ship speed, g is the gravitational constant, and L is the characteristic length which, in the case of Holtrop and Mennen, is the waterline length, L_{wl}, and in the case of Hollenbach, is the characteristic length, L_c. The Holtrop & Mennen method is applicable for $Fr \leq 0.45$. The Froude number limit for the Hollenbach method is dependent upon the type of ship and length;

$$Fr_{max} = g_1 + g_2 L_{bp} + g_3 L_{bp}^2 \tag{20}$$

where the coefficients are listed in Table VI.

The lower bound on ship speed for the fuel oil consumption calculations is set to the ship speed achievable at 25% of the SMCR (specified maximum continuous rating) of the engine, since extrapolation of our estimate of engine performance is unreliable below 25% engine load. If engine data at a lower

	single screw design draft	single screw ballast draft	twin screw design draft
g_1	0.642	0.42	0.83
g_2	-0.635	-0.20	-0.66
g_3	0.15	0.0	0.0

TABLE VI: Coefficients for Froude number limit for Hollenbach [1]

engine load is provided as an input to the program, the lowest load for which data is provided becomes the lower bound on ship speed for fuel oil consumption calculations. The upper limit on speed is restricted to 110% of the SMCR since the engine is not designed to run above 110% engine load.

The propeller cavitation limit of 10% back cavitation can also place an upper limit on the ship speed. While no other limit is explicitly placed on speed by the propeller calculations, an inefficient propeller can cause a limit on maximum speed realized through the engine calculations. If the propeller is designed by the code, a propeller is selected that maintains a reasonable efficiency through the full range of operations. If the propeller design is based on values input by the user and the propeller efficiency for some reason is very low, the limit on speed is realized in the engine calculation portion of the code because the brake power required will be very high.

IX. Performance Improvements

A. Engine Modifications

Both Wärtsilä and MAN B&W offer several tuning options for their diesel engines which reduce specific fuel oil consumption at certain engine loads, usually at the expense of greater specific fuel oil consumption at other loads. Carbon production is directly and linearly correlated with fuel consumption; however, NOx production is correlated with temperature and thus can increase with improved fuel consumption. These competing tendencies must be balanced to meet regulatory requirements.

Changes to the SFOC can be accomplished through various engine tuning methods such as exhaust gas bypass, variable turbine area, electronic control tuning and turbocharger cut-out, each of which can be tuned for partial load (50-85% of SMCR) or low load (25-70% of SMCR). Changes to the SFOC for each tuning method can be applied to the SFOC values determined in Section VII. These methods will typically reduce SFOC at lower engine load ranges while increasing SFOC at higher engine loads. Methods cannot be combined for further fuel consumption improvements.

a) Delta or Electronic Control Tuning (ECT): ECT, also known as Delta tuning, is the adjustment of exhaust valve and injection timing using the electronic controls of the engine to optimize performance at a lower engine load. This tuning method can be applied to any engine with electronic controls (as opposed to camshaft-controlled engines), and does not require any additional equipment or engine component modifications, including turbochargers. Figure 12 provides an example change in engine SFOC with ECT compared to generic SMCR tuning; these values are the default used by the program if specific data pertinent to the selected engine are not available.

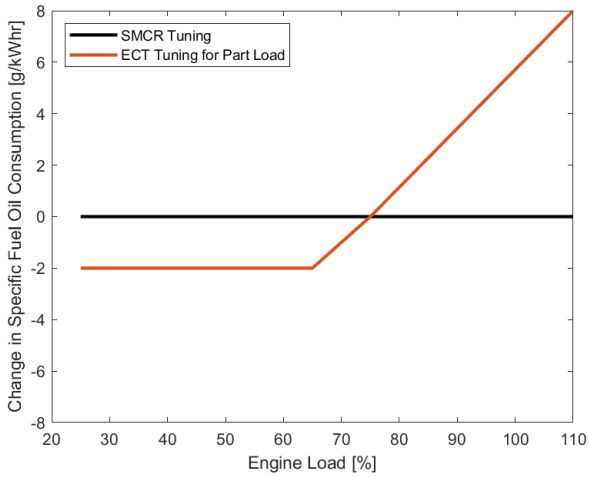

Fig. 12: Change in Specific Fuel Oil Consumption (SFOC) as a function of Engine Load for electronic control tuning (ECT).

b) Variable Turbine Area (VT or VTA): VTA regulates the exhaust gas pressure in order to precisely match the amount of air to the quantity of injected fuel at all points in an engine's load and speed range. The result is reduced specific fuel consumption, reduced emissions of hydrocarbons and carbon dioxide and improved engine response. VTA requires the replacement of the fixed-vane nozzle rings in standard turbochargers with a nozzle ring equipped with adjustable vanes; altering the pitch of the vanes adjusts the air flow. Figure 13 provides an example change in engine SFOC with VTA compared to SMCR tuning; these values are the default used by the program if specific data pertinent to the selected engine are not available.

c) Bypass or Exhaust Gas Bypass (EGB): EGB allows the use of smaller turbochargers which have higher efficiencies at lower engine loads. To prevent over-speeding of the turbocharger at high engine loads, an exhaust gas bypass is installed which routes some exhaust gas around the turbocharger at high engine loads. This has the added advantage of increasing exhaust gas temperatures at high loads. EGB requires the installation of an exhaust gas bypass system and, possibly, replacement of the turbochargers. Figure 14 provides an example change in engine SFOC with EGB compared to SMCR tuning; these values are the default used by the program if specific data pertinent to the selected engine are not available.

d) Turbocharger Cut-Out (TCCO): TCCO is the blanking of one or more turbochargers at low engine loads, either manually or automatically, to improve efficiency at low loads. Savings depend on the general set up of the engine and the number of turbochargers applied. This method requires installation of a blanking device and is applicable to any engine with multiple turbochargers. Figure 15 provides an example

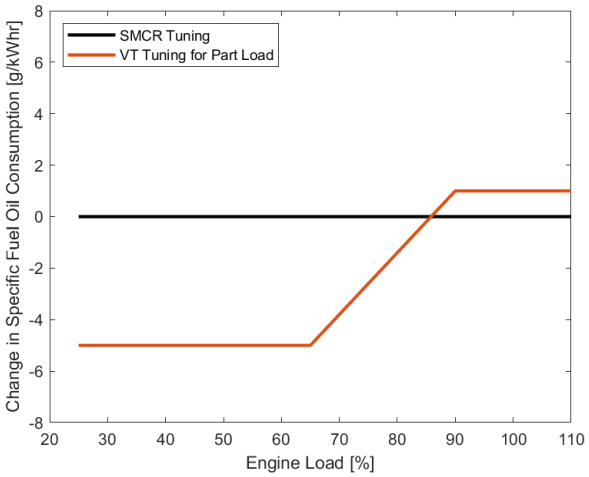

Fig. 13: Change in Specific Fuel Oil Consumption (SFOC) as a function of Engine Load for variable turbine area (VTA).

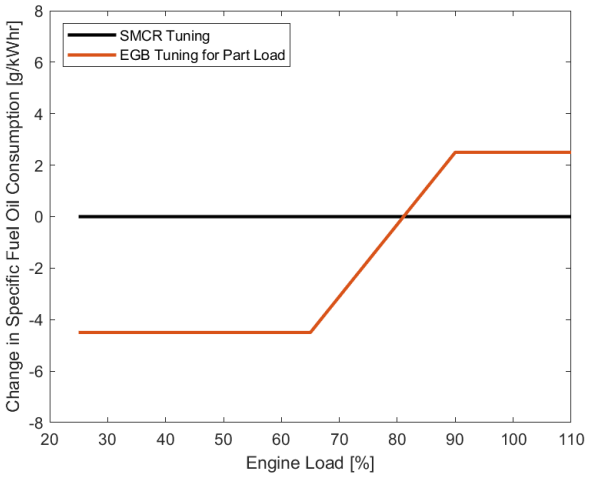

Fig. 14: Change in Specific Fuel Oil Consumption (SFOC) as a function of Engine Load for exhaust gas bypass (EGB).

change in engine SFOC with turbocharger cut-out compared to SMCR tuning; these values are the default used by the program if specific data pertinent to the selected engine are not available.

B. Propeller Optimization

The propeller optimization code described in this section is employed when the propeller specifications are not provided in the input data or when a new propeller is desired. The necessary parameters for propeller design using the Wageningen series are number of blades, diameter, pitch-to-diameter ratio (P/D), expanded area ratio (AE/AO) and design speed. If desired, a maximum speed, greater than design speed, may

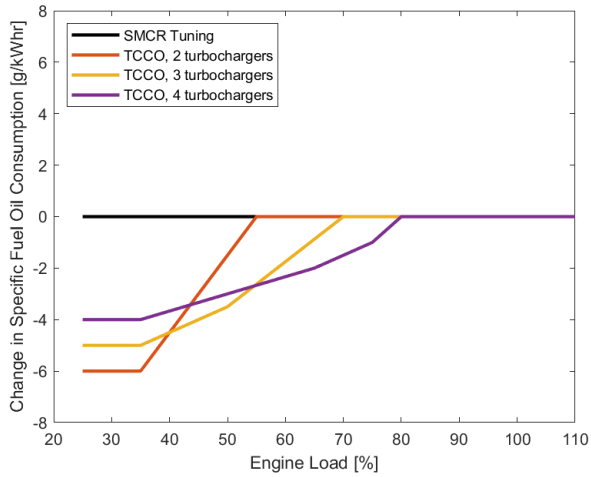

Fig. 15: Change in Specific Fuel Oil Consumption (SFOC) as a function of Engine Load for turbocharger cut-out (TCCO) for various numbers of turbochargers.

be entered to ensure cavitation-free operation above the design speed.

Using the number of blades and diameter input by the user, we select an expanded area ratio using equation (17), then calculate K_T, K_Q and open water efficiency for a range of pitch to diameter ratios (P/D) using the Wageningen equations, presenting a family of appropriate propeller curves. The propeller operating point at design speed is determined for each P/D ratio using the J determined by the intersection of $(K_T/J^2)J^2$ for the ship and K_T for the propeller as shown in Figure 16, following the procedure described in Section VI.

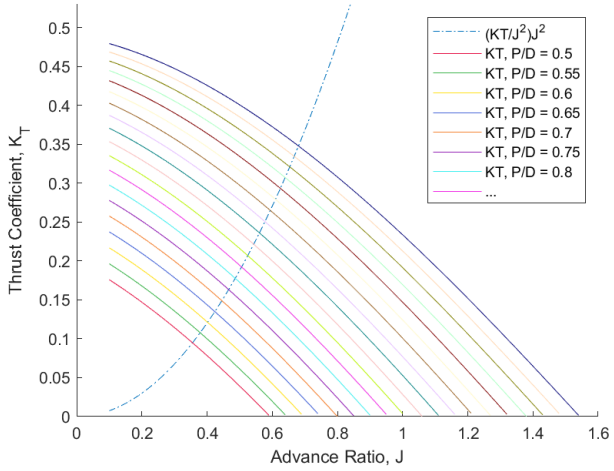

Fig. 16: Intersection of $(K_T/J^2)J^2$ for ship with K_T for propellers at various P/D ratios.

This matrix of P/D values is carried through the engine

efficiency calculation, at which point the optimum P/D, that which produces the lowest fuel consumption at design speed when operated in conjunction with the engine, is selected. Note that the propeller with the highest open water propeller efficiency is not necessarily the most efficient overall choice for a propeller design, because the resulting propeller operating speed may force the engine into a less efficient operating point; therefore, the propeller that results in the best specific fuel oil consumption is selected.

An example is shown in Figure 17. The engine brake power/speed point for a range of pitch-to-diameter ratios is plotted against the engine layout diagram. Only those P/D ratios that fall within the diagram are considered for use; of those, the one selected is the P/D ratio that provides the lowest specific fuel oil consumption. Note that in this example, this is not the one with the highest propeller efficiency.

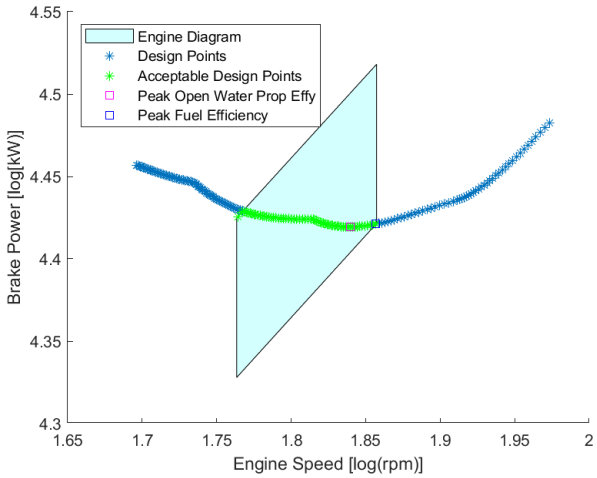

Fig. 17: Optimum propeller design selection.

It is possible that the SMCR point does not fall within the engine layout diagram. The can happen if, for example, reducing design speed or installing an energy saving device causes the brake power at design speed to be well below the engine layout diagram for the originally installed engine. In these instances, we project the propeller curve until it intersects the engine layout diagram and pick that intersection point as the SMCR; in such cases, the design speed will occur at an engine power level lower than 100%. For example, the top plot in Figure 18 presents a case in which the design speed with engine margin and sea margin still falls below the engine load diagram; in this case, design speed in heavy running can be achieved at 86% of SMCR (86% engine load).

In cases where the design speed falls above the engine load diagram, it may not be possible to achieve design speed at heavy running with the currently designed propeller and engine combination. The disparity could be due to a number of causes, e.g. incorrect ship data resulting in a high estimate of resistance, incorrect propeller data resulting in an inefficient propeller design, or high sea or engine margins. See, for

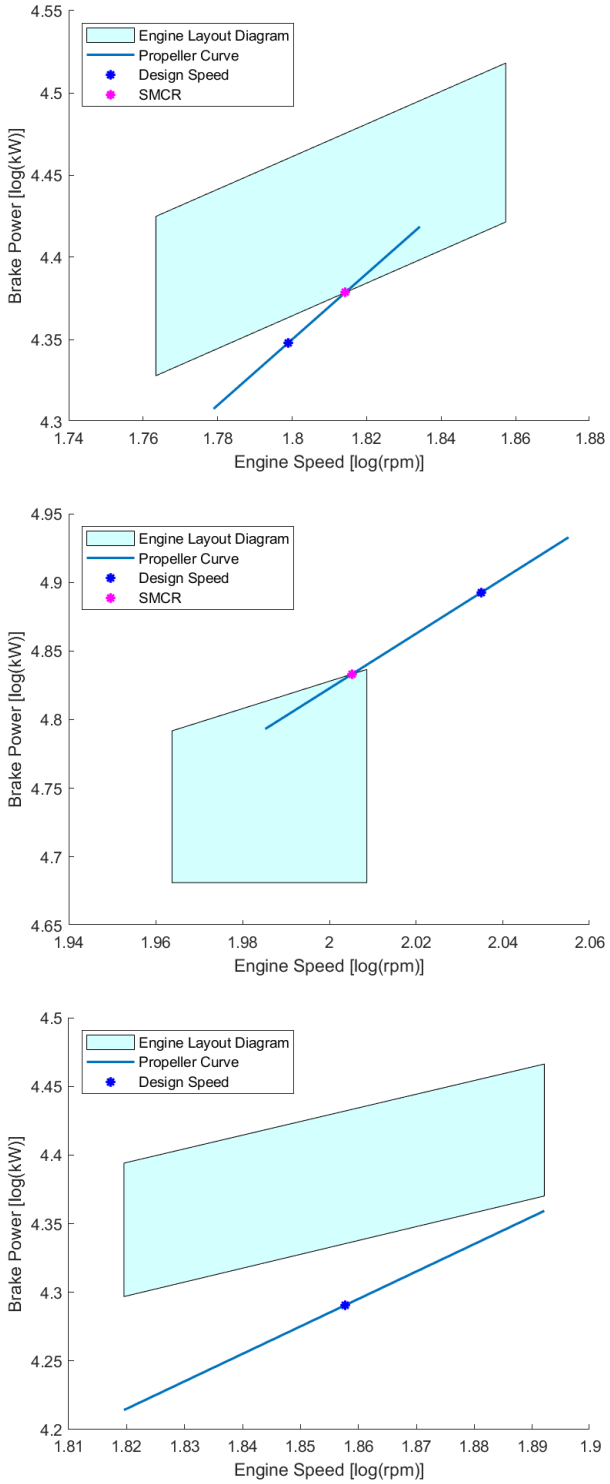

Fig. 18: SMCR selection in which design speed falls outside the engine load diagram. Low power (top), high power (middle), and no intersection (bottom).

example, the center image in Figure 18, in which design speed occurs at 112% of SMCR.

Occasionally, the propeller curve will not intersect the engine layout diagram at all; see, for example, the bottom image in Figure 18. The program will return an error; it is left to the user to select the proper remedy by either allowing the program to select a propeller instead of inputting propeller specifications, or by increasing propeller margin to shift the curve to the left or decreasing propeller margin to shift the curve to the right. In the example shown at the bottom of Figure 18, increasing the propeller margin to 6% from 5% will cause the propeller curve to intersect the engine load diagram.

C. Bulbous Bow Removal

A properly designed bulbous bow reduces propulsion power at and around the designed operating speed of the ship. When a ship is operated at a speed significantly different from the speed for which the bulb was designed, the bulb can have an adverse effect on the resistance of the ship, increasing propulsion power and, thus, fuel consumption. This variation in the impact of the bulbous bow is shown in Figure 19 from Carlton [5], who states that the positive impact of bulbous bows occurs over a narrow range of ship speeds, so they are usually employed in ships that operate at clearly defined speeds for much of their time. If a ship is operated consistently off-design, e.g. due to a new operational profile, it may be cost effective to modify the bulb's shape or to remove the bulb entirely.

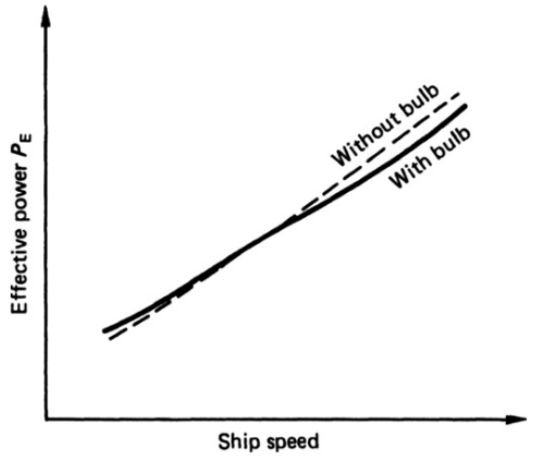

Fig. 19: Bulb impact over a range of speeds [5]

Recalling equation (3), the only characteristics of the bulb that are used by Holtrop and Mennen to calculate the impact of the bulb on the ship performance are the area and centroid of the transverse cross-section of the bulb at the forward perpendicular; a small set of data to capture a widely varying possible performance impact from a bulbous bow. Further, the only characteristic of the bulb that is used by Hollenbach is the length of the bulb forward of the forward perpendicular, and even smaller set of data. Thus, either estimate is merely a rough approximation of the impact of the bulb on the performance of the ship. *Since this approximation is so rough, any indication from these calculations that bulb removal may be beneficial is merely a recommendation for further study with more detailed analysis of the specific bulb installed in the ship.*

1) Ship Properties with Bulb Removed: Removing the bulbous bow reduces the volume, displacement and wetted surface area of the hull, and thus has a small impact on the lcb location and the block coefficient as well. The following is a description of the process for calculating the impact of bulb removal.

Assuming the bulb is approximately a half-ellipsoid, the bulb volume, ∇_b is calculated as:

$$\nabla_b = \frac{2}{3} A_{bt} L_b$$

where A_{bt} is the transverse cross-sectional area of the bulb at the forward perpendicular and L_b is the bulb length forward of the forward perpendicular. The bulb surface area is approximated using

$$A_b = 2\pi \Big(\frac{(\pi A_{bt})^{1.6} + 2(L_b \sqrt{\pi A_{bt}})^{1.6}}{3} \Big)^{(1/1.6)}.$$

The wetted surface area of the ship without a bulb, A_{wsnb}, is thus merely

$$A_{wsnb} = A_{ws} - A_b,$$

assuming that the remaining ship structure is reshaped to form the bulb-less bow.

The volume of the ship without the bulb, ∇_{nb}, is

$$\nabla_{nb} = \nabla - \nabla_b,$$

and the displacement of the ship without the bulb, Δ_{nb}, is

$$\Delta_{nb} = \rho \nabla_{nb}.$$

The longitudinal center of buoyancy of the ship without a bulb, lcb_{nb}, is slightly aft of the original lcb due to the removal of volume forward, thus

$$lcb_{nb} = \frac{lcb\nabla - lcb_b \nabla_b}{\nabla_{nb}}$$

where the longitudinal center of buoyancy of the bulb, lcb_b, measured from the aft perpendicular, is

$$lcb_b = L_{bp} + \frac{4L_b}{3\pi}$$

assuming that the bulb is a half-ellipsoid.

The change in draft is negligible since the buoyancy of the bulb relative to the buoyancy of the entire ship is small, and, further, this small loss in buoyancy is partially offset by a reduction in weight due to steel that is removed. For example, a sample container ship bulb displaces 330 tonnes of seawater; with a 120 tons/cm immersion at design draft, removal of the bulb results in less than a 3 cm change in draft without accounting for the change in ship weight due to removal of the steel in the bulb.

Bulb removal does not change L_{bp} or B and change to T is negligible, so there is a very small change in block coefficient, C_b, which is recalculated to be

$$C_b = \frac{\nabla_{nb}}{L_{bp} B T}$$

2) Holtrop & Mennen: After recalculating the above properties of the now bulb-less ship, we eliminate the reduction to wave resistance in Holtrop & Mennen due to the presence of a bulbous bow by setting the A_{bt} and h_b values to zero. At this point, the resistance, propeller and engine calculations are run using the new bulb-less ship properties to determine the power and fuel required for an equivalent ship with the bulb removed.

3) Hollenbach: In Hollenbach's calculations, the impact of the bulbous bow is accounted for solely by increasing the ship length to include the length of the bulb. In order to measure the impact of eliminating the bulbous bow, one does not get reasonable results by merely decreasing the length of the ship by the amount of bulb removed and decreasing the surface area by the surface area of the removed portion of the bulb, because the resulting calculation indicates an increased resistance over the full range of ship speeds, rather than the expected profile shown in Figure 19.

To estimate the impact of the bulb, we use the formulation proposed by Kracht [13], who employs a residual power reduction coefficient, $\Delta C_{P\nabla R}$, to capture the change in residual resistance for a ship with and without a bulb,

$$\Delta C_{P\nabla R} = 1.0 - C_{Rwith}/C_{Rwithout}, \tag{21}$$

where C_{Rwith} and $C_{Rwithout}$ are residual resistance coefficients of equivalent ships with and without a bulb. Figure 53 shows the variation of $\Delta C_{P\nabla R}$ with Froude number for various bulb shapes and baseline hulls.

We assume, for any ship using the Hollenbach formulation, that the maximum $\Delta C_{P\nabla R}$ is equal to 0.25 and occurs at the design speed. Further, the $\Delta C_{P\nabla R}$ is assumed to be parabolic with a minimum value of zero occurring at the point in which residual resistance becomes nonlinear.

To apply this assumption, we first calculate Hollenbach's residual resistance for the ship with the bulb. We then find the inflection speed at which the residual resistance changes from linear to higher order and apply a correction such that $\Delta C_{P\nabla R} = 0.0$ at the inflection speed and changes in a parabolic form to a maximum of $\Delta C_{P\nabla R} = 0.25$ at design speed, then decreases above design speed, again parabolically. $\Delta C_{P\nabla R}$ is constrained to always be non-negative. The remainder of the resistance elements are calculated using updated values for the bulb-less ship. Figure 20 shows a calculation for a ship with a bulb shown in dotted lines and without the bulb shown in solid lines. Note that the residual resistance without the bulb is higher than the residual resistance with the bulb at higher speeds. The frictional resistance is lower for the ship without the bulb through the full speed range. The total resistance is slightly lower at low speed and higher at high speeds.

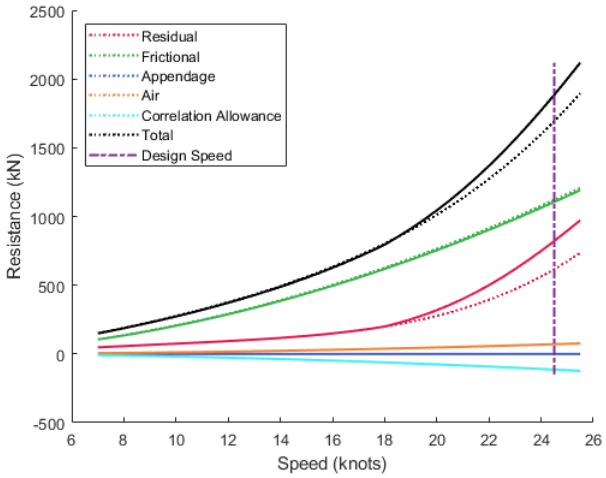

Fig. 20: Resistance calculations using Hollenbach. Ship with bulb shown in dotted lines; ship without bulb shown in solid lines.

D. Energy Saving Devices

A variety of energy saving devices can be implemented which, in general, have the effect of modifying flow into or out of the propeller in a manner that improves efficiency through some range of speeds. Examples include propeller boss cap fins, ducted propellers, pre-swirl stators and asymmetric rudders or hulls, among others.

One potential fuel-saving technology is the Mewis duct, which is advertised to achieve a fuel savings in the neighborhood of 5 to 7 percent, depending on the thrust coefficient, C_{th}, of the original vessel,

$$C_{th} = \frac{T_o}{\frac{1}{2}\rho\pi\frac{D^2}{4}(V_a)^2}$$

where T_o is thrust and V_a is the water speed at the propeller.

Since the ship data provided to this program is not particularly detailed, it is not possible to accomplish a full CFD-scale simulation of the Mewis duct; further, we do not have the information necessary to properly modify the wake fraction, w, thrust deduction factor, t, and relative rotative efficiency, η_r for a ship with a Mewis duct installed. Therefore, the process used to estimate the impact of the Mewis duct is to calculate the ship's thrust coefficient using the standard thrust value, then use the plot shown in Figure 21 to determine a power reduction that is applied to the brake power. Mewis and Guiard [7] also report a slight increase in propeller rotation rate on the order of 1%, so the propeller rotation rate is increased by 1% as well. These modifications to delivered power and rpm are applied before the engine SFOC calculations.

Per [17], impact of the Mewis Duct is even greater in ballast than in loaded condition. For example, the average of 35 model tests with and without a Mewis Duct show an average of a 5.7% power reduction at design draft, and a 7.3% power reduction at ballast draft. We do not currently include this increased impact.

X. Data Estimates and Calculations

The program described herein requires a bare minimum of essential data in order to estimate ship performance and

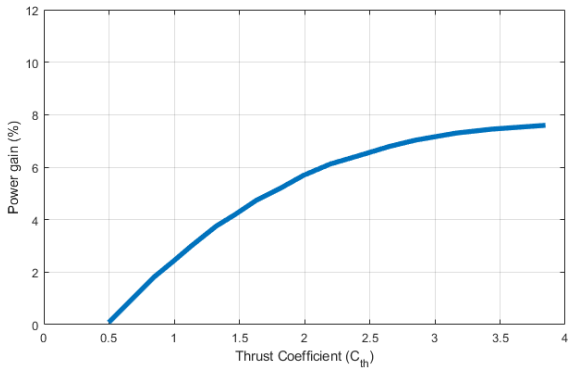

Fig. 21: Power savings claimed by the Mewis duct, as a function of thrust coefficient, C_{th}, per [7].

potential energy savings; however, the predictions improve greatly with additional data provided. This section describes the methodologies for estimating any missing input data and cites the sources for the estimates.

A. Displacement

If displacement at design draft is not entered, it can be estimated from deadweight, DWT, as [16]

$$\Delta = k_\Delta DWT$$

where $k_\Delta = 1.17$ for tankers and bulkers, and $k_\Delta = 1.33$ for container ships.

If displacement at ballast condition, Δ_B, is not provided, then it is estimated from displacement at design draft using

$$\Delta_B = \Delta - \rho C_{wp} B L_{wl} (T - T_B)$$

where where T is mean draft at design draft, T_B is mean draft at ballast, and C_{wp} is the waterplane coefficient. We place a lower limit on this calculation such that ballast displacement must be a minimum of 10% of displacement at design draft.

B. Length

Length at the waterline, L_{wl}, and length between perpendiculars, L_{bp}, are both required. If neither is provided, then we estimate L_{wl} as [16]

$$L_{wl} = 0.956 L_{oa}$$

where L_{oa} is length overall.

The difference between L_{wl} and L_{bp} is the distance from the aft perpendicular to the aftmost point of the wet hull, d_{ap},

$$L_{wl} = L_{bp} + d_{ap}.$$

If L_{wl} and L_{bp} are not provided and d_{ap} is not available, the relationship between L_{wl} and L_{bp} can be estimated as [14]

$$L_{wl} = k_{ll} L_{bp}$$

where $k_{ll} = 1.01$ for tankers and bulkers and $k_{ll} = 1.02$ for container ships.

C. Block Coefficient

Block Coefficient, C_b, is defined as the volumetric displacement of the ship divided by the volume of the bounding box around the wetted hull

$$C_b = \frac{\nabla}{L_{wl} B T}. \tag{22}$$

Note that the volumetric displacement and mean draft must correspond with one another; we expect both to be at design draft.

Per [16], block coefficients for tankers and bulkers range 0.80 - 0.85, and for container ships range from 0.50 - 0.70. We assume $C_b = 0.8$ for tankers and bulkers, and $C_b = 0.6$ for container ships if the appropriate dimensions are not provided by the user.

D. Beam

If beam, B, is not provided, we calculate beam from the block coefficient, length and draft using (22).

E. Midship Section Coefficient

The midship section coefficient, C_x, is defined as the midship section area, A_x, divided by the bounding box of that area,

$$C_x = \frac{A_x}{BT}.$$

If C_x is not provided by the user, then we estimate it using [1]

$$C_x = \frac{1}{1 + (1 - C_b)^{3.5}}.$$

F. Waterplane Area Coefficient

The waterplane area coefficient, C_{wp}, is defined as the area of the waterplane, A_{wp}, divided by the bounding box of that area,

$$C_{wp} = \frac{A_{wp}}{L_{wl} B}.$$

If C_{wp} is not provided, we estimate it using [1]

$$C_{wp} = k_{wp1}(C_p + k_{wp2});$$

where $k_{wp1} = 0.763$ and $k_{wp2} = 0.34$ for tankers and bulkers with $0.56 < C_p < 0.87$, and $k_{wp1} = 3.226$ and $k_{wp2} = -0.36$ for container ships with $0.57 < C_p < 0.62$; otherwise, C_{wp} is assumed to equal 0.907.

G. Wetted Surface Area

If the wetted surface area, A_{ws}, is not provided, we use Mumford's formula as modified by Kristensen and Lützen [14]

$$A_{bh} = k_{ws}(\frac{\nabla}{T} + 1.9 L_{wl} T)$$

where $k_{ws} = 0.990$ for tankers and bulkers and $k_{ws} = 0.995$ for container ships. This surface area, A_{bh}, describes the bare

hull only; to this we add an estimate for wetted surface of appendages

$$A_{app} = 0.7T + 0.015L_{wl}$$

so that

$$A_{ws} = A_{bh} + A_{app}.$$

If wetted surface area is not provided but appendage surface areas are provided in the input data, the input appendage surface areas are ignored and the estimate above is used instead.

If the wetted surface area in ballast, A_{wsB}, is not provided, then it is estimated from wetted surface at design draft using [1]

$$A_{wsB} = A_{ws} - k_b(T - T_B)(L_{wl} - B)$$

where T is mean draft at design draft, T_B is mean draft at ballast, and $k_b = 2.0$ for tankers and bulkers and $k_b = 2.4$ for container ships.

H. Longitudinal Center of Buoyancy

If the distance of the longitudinal center of buoyancy from the aft perpendicular, lcb_{ap}, is not provided, we use Guldhammer and Harvald's estimate of the best possible lcb location, given as a percentage of waterline length forward of the mean of the waterline [8]

$$lcb = 9.4 - 43.8Fr_{des}$$

where Fr_{des} is the Froude number at design speed.

I. Transverse Area Exposed to Wind

The transverse area exposed to wind, A_{exp}, is the transverse cross-sectional area of the hull and superstructure, including cargo, above the design waterline. This area is in a plane orthogonal to forward motion. Note that a common mistake is to provide the longitudinal windage area, which is the area used to determine heel caused by wind in stability calculations; this value is too large and will result in a very high wind resistance. If A_{exp} is not provided, we estimate it to be

$$A_{exp} = BT.$$

If area exposed to wind at ballast, A_{expB}, is not provided, we assume that the exposed area at design draft is increased by the change in trim forward multiplied by the beam:

$$A_{expB} = A_{exp} + (T_{fB} - T_f)B$$

where T_{fB} is trim forward at ballast.

J. Propeller Diameter

It is strongly encouraged that the propeller diameter, D, be provided by the user. If unavailable, we estimate propeller diameter using [14]

$$D = k_{d1}T + k_{d2}$$

where $k_{d1} = 0.395$ and $k_{d2} = 1.30$ for tankers and bulkers, and $k_{d1} = 0.623$ and $k_{d2} = -0.16$ for container ships.

K. Propeller Hub Depth

The depth of the center of the propeller hub, h, can be estimated as

$$h = T - D/2.$$

L. Thrust Deduction Factor

We use Holtrop's equation to estimate t for single-screw vessels as [1]

$$t = \frac{0.25014\left(\frac{B}{L_{wl}}\right)^{0.28956}\left(\frac{\sqrt{BT}}{D}\right)^{0.2624}}{(1 - C_p + 0.0225lcb)^{0.01762}} + 0.0015C_{stern}$$

For twin-screw vessels [1],

$$t = 0.325C_b - \frac{0.1885D}{\sqrt{BT}}.$$

In general, t is a small positive number somewhere around 0.2. We limit the thrust deduction factor to the range of 0.1 to 0.25.

The thrust deduction factor at ballast, t_B can be determined using [18]

$$\frac{(1 - t_B)}{(1 - t)} = 1 + \left[\frac{T_B}{T} - 1\right](0.4322 + 0.4880C_b).$$

M. Taylor Wake Fraction

The wake fraction, w, accounts for differences in the propeller inflow between the propeller in open water and the propeller behind the hull; w depends on the shape of the hull and the propeller location and size. We calculate wake fraction using a formula from Holtrop & Mennen [1], for a single-screw vessel

$$\begin{aligned} w &= C_9C_v\frac{L_{wl}}{T_a}\left(0.0661875 + 1.21756C_{11}\frac{C_v}{1 - C_{P1}}\right) \\ &+ 0.24558\sqrt{\frac{B}{L_{wl}(1 - C_{P1})}} - \frac{0.09726}{0.95 - C_p} \\ &+ \frac{0.11434}{0.95 - C_b} + 0.75C_{stern}C_v + 0.002C_{stern} \end{aligned}$$

where

$$\begin{aligned} C_8 &= (BA_{ws})/(L_{wl}DT_a) && \text{for } B/T_a \le 5 \\ C_8 &= A_{ws}(7(B/T_a) - 25)(L_{wl}D(B/T_a - 3)) && \text{for } B/T_a > 5 \end{aligned}$$

$$\begin{aligned} C_9 &= C_8 && \text{for } C_8 \le 28 \\ C_9 &= 32 - 16/(C_8 - 24) && \text{for } C_8 > 28 \end{aligned}$$

$$\begin{aligned} C_{11} &= T_a/D && \text{for } T_a/D \le 2 \\ C_{11} &= 0.0833333(T_a/D)^3 + 1.33333 && \text{for } T_a/D > 2 \end{aligned}$$

$$C_{P1} = 1.45C_p - 0.315 - 0.0225lcb$$

and the viscous resistance coefficient, C_v, is

$$C_v = (1+k)C_f + C_a + C_{app}.$$

Recall that $(1+k)$ is the form factor, C_f is the coefficient of frictional resistance, C_a is the correlation allowance, and C_{app} is the coefficient of frictional resistance for appendages.

For a twin-screw vessel, the wake fraction is estimated using

$$w = 0.3095C_b + 10C_vC_b - 0.23\frac{D}{\sqrt{BT}}.$$

For single screw ships, wake fraction is normally in the range of 0.2 to 0.45, with large block coefficient ships having relatively large wake fractions. We limit the wake fraction to the range of 0.1 to 0.5.

Per [18], wake fractions in ballast tend to be 5-15% higher than wake fraction in the loaded condition, resulting in a larger hull efficiency. The revised wake fraction at ballast, w_B, can be determined as [18]

$$\frac{(1-w_B)}{(1-w)} = 1 + \left[\frac{T_B}{T} - 1\right](0.2882 + 0.1054\Theta)$$

where $\Theta = (100\cdot$ trim by bow$)/L_{bp}$ is the trim angle. Trim by the bow is measured in meters and will typically be a negative number at ballast.

N. Relative Rotative Efficiency

Relative rotative efficiency, η_r, accounts for differences in performance of the propeller behind the hull other than those dealt with by the wake fraction and the thrust deduction, and is generally near unity; typical values range from 0.96 to 1.04. We estimate η_r using Holtrop & Mennen's recommendation referenced in [1] of

$$\eta_r = 0.9922 - 0.05908(AE/AO) + 0.07424(C_p - 0.0225lcb)$$

for single-screw vessels and

$$\eta_r = 0.9737 + 0.111(C_p - 0.0225lcb) - 0.06325(P/D)$$

for twin-screw vessels. Values are limited to a range of 0.95 to 1.05.

O. Expanded Area Ratio

As stated in Section IX-B, the propeller expanded area ratio, AE/AO, is estimated based on cavitation considerations if it is not provided by the user. The initial rough estimation uses an equation proposed by Keller and referenced in [1]:

$$\frac{AE}{AO} = \frac{(1.3 + 0.3Z)Th}{(p_0 - p_v)D^2} + K$$

where Th is thrust at design speed, p_0 is the hydrostatic pressure at the centroid of the propeller hub, p_v is the saturation pressure of the water which equals 2,291 Pa at 20^{o}C, D is the propeller diameter, and the constant K is

$$\begin{aligned} K &= 0.2 \quad \text{for single-screw vessels} \\ K &= 0.1 \quad \text{for slow twin-screw vessels} \\ K &= 0.0 \quad \text{for fast twin-screw vessels.} \end{aligned}$$

For the purposes of our code, slow is defined as 20 knots or less and fast is greater than 20 knots. Thrust, Th, is calculated as

$$Th = \frac{R_{hrDes}}{(1-t)}$$

where R_{hrDes} is the heavy-running resistance at design speed and t is the thrust deduction factor. Hydrostatic pressure, p_0, is

$$p_0 = P_{atm} + \rho gh$$

where ρ is seawater density, g is the gravitational constant, and h is the draft of the centroid of the propeller hub. Note that the full propeller calculation includes a further check on cavitation and, if cavitation levels are exceeded, AE/AO is increased until cavitation requirements are met.

P. Default Values

A few parameters have default values included in the program, which are implemented if no values are provided by the user. These defaults include the following:

- Engine margin, $em = 10\%$
- Sea margin, $sm = 15\%$
- Propeller margin, $pm = 5\%$
- Transmission efficiency, $\eta_s = 99\%$
- Number of propellers = 1
- Number of propeller blades, $Z = 4$

XI. Examples

In this section we provide examples of a very large crude carrier (VLCC), a product tanker, and a container ship. Where available, we provide data from the actual ship test data or operational data and compare to our calculations. Input data can be seen in Table VII.

A. Very Large Crude Carrier (VLCC)

The first example ship is a VLCC. We begin with the resistance calculation using Holtrop & Mennen; results are presented in Figure 22. The majority of the speed range is in the regime dominated by frictional resistance.

The calculated input values for the propeller module are shown in Figure 23. Since the pitch/diameter ratio (P/D) was not provided, the program calculated the P/D to be 0.76 to achieve the minimum specific fuel oil consumption as shown in Figure 24. The resulting propeller curves, shown in Figure 25, generate the open water efficiency shown in Figure 26. Cavitation limits are well above design speed as shown in Figure 27.

The resultant brake power for trial conditions is presented in Figure 28 along with sea trial and log data corresponding to trial condition. The percent difference between the log data and the estimate ranges from 0.3 to 6.2 percent, with the majority being within five percent; see Table VIII. Brake power versus rotation rate is shown in Figure 29.

The engine diagram with SMCR and CSR including corresponding shop test data is shown in Figure 30; test data show excellent correlation with program estimates. Figure 31

TABLE VII: Input data for example vessels

Ship Name	VLCC	Container	Product Tanker
	hullform data		
ship type	tanker	container	tanker
bulbous bow	no	yes	yes
energy-saving device	no	no	no
design speed (knots)	15.6	25.2	14.9
max speed for cavitation limit (knots)	–	–	–
LBP (m)	324	334	174
LWL (m)	330	333	–
LOA (m)	–	–	183
Beam (m)	60	45.6	32.2
Design draft forward (m)	20.5	13	11.1
Design draft aft (m)	20.5	13	11.1
Displacement at Design Draft (tonnes)	332503	127968	50786
DWT (tonnes)	286512	–	–
LCB to AP (m)	173	161	–
AP to aftmost point of wet hull (m)	7	–	–
wetted surface area (m^2)	28022.8	17734.6	–
transverse area above water (m^2)	1227	1830	608.4
ballast draft forward (m)	8	–	–
ballast draft aft (m)	11	–	–
displacement at ballast (tonnes)	–	–	–
LCB to AP at ballast (m)	–	–	–
wetted surface at ballast (m^2)	–	–	–
area above water at ballast (m^2)	–	–	–
midship section coefficient	0.999	0.9853	–
water-plane coefficient	0.907	0.8025	–
block coefficient	0.816	0.6297	0.7981
longitudinal prismatic coefficient	0.817	0.6391	–
bulb length from FP (m)	–	12	–
transverse sectional area of bulb (m^2)	–	38	–
vertical centroid of bulb area (m)	–	7.6	–
bulb surface area (m^2)	–	–	–
bulb volume (m^3)	–	–	–
	appendage surface areas (m^2)		
rudder behind skeg	–	–	–
rudder behind stern	270	–	–
twin screw rudder (slender)	–	–	–
twin screw rudder (thick)	–	–	–
skeg	–	–	–
shaft brackets	–	–	–
strut bossing	–	–	–
hull bossing	–	–	–
exposed shafts	–	–	–
stabilizer fins	–	–	–
dome	–	–	–
bilge keels	–	–	–
	engine data		
engine make	MAN	Wärtsilä	MAN
engine model	G80ME-C9-2	RTA96C	S50ME-C8-2
engine control	Electronic	Electronic	Electronic
number of cylinders	7	12	6
number of turbochargers	–	–	–
	propeller data		
number of props	1	1	1
diameter (m)	10.6	8.8	6
propeller height above baseline (m)	15	–	–
number blades	4	6	4
expanded area ratio	0.4	0.95	0.5411
pitch/ diameter ratio at 0.7R		0.9895	0.6778
	margins		
engine margin	0.2	0.1	0.1
sea margin	0.15	0.15	0.15
shaft efficiency	0.99	0.99	0.99
propeller margin	–	–	–

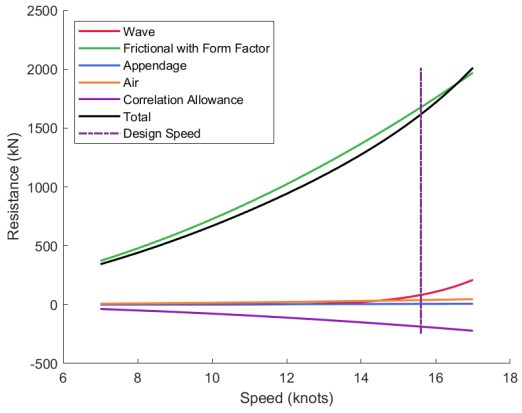

Fig. 22: Resistance calculation results for the example VLCC. For this ship operating below the design speed of 15.6 knots, the ship resistance is dominated by frictional resistance.

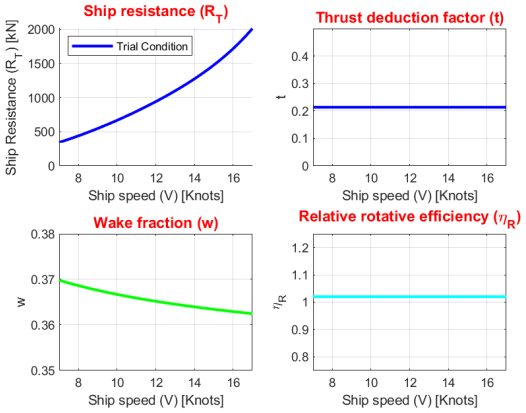

Fig. 23: Calculated propeller input for the example VLCC.

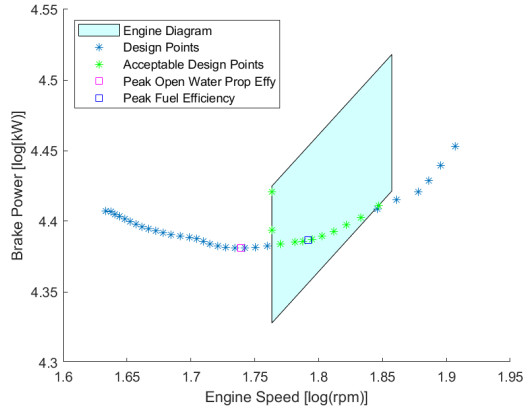

Fig. 24: Pitch to diameter selection for the example VLCC. The peak fuel efficiency point is selected, shown as a blue square.

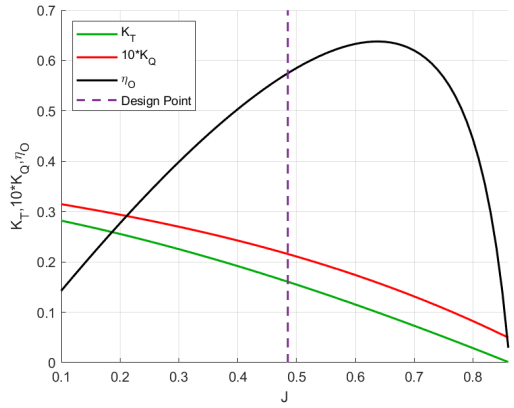

Fig. 25: Calculated propeller curves for the example VLCC, plotted as a function of advance ratio, J.

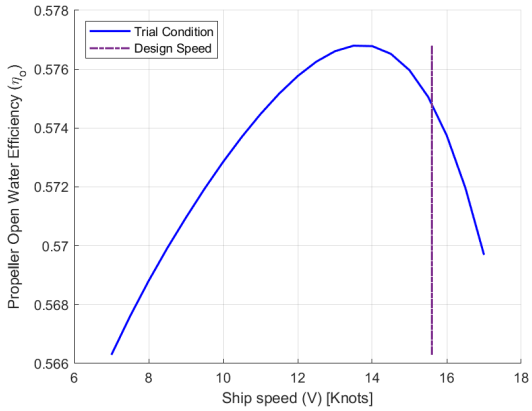

Fig. 26: Propeller open water efficiency at trial condition for the example VLCC as a function of ship speed.

TABLE VIII: Comparison of calculated values to ship measurement data from sea trials and operational logs for the example VLCC brake power in MW at trial condition, as shown in Figure 28.

Speed [kt]	Calculated [MW]	Data [MW]	% Difference
9.38	3.987	4.157	-4.1
10.25	5.135	5.346	-3.9
10.63	5.697	5.904	-3.5
11.01	6.300	6.717	-6.2
11.54	7.211	7.576	-4.8
12.00	8.072	8.532	-5.4
12.50	9.090	9.281	-2.1
13.00	10.201	10.713	-4.8
13.69	11.909	11.950	-0.3
15.51	17.716	17.900	-1.0
16.17	20.545	20.402	0.7
16.45	21.851	21.715	0.6

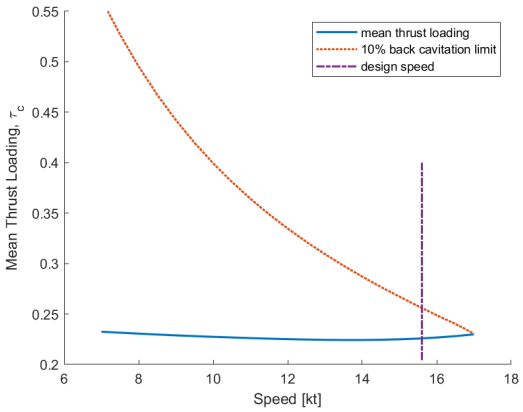

Fig. 27: Propeller cavitation limits for the example VLCC. Propeller performance is inhibited by cavitation wherever the mean thrust loading exceeds the 10% back cavitation limit. For this vessel, this occurs at approximately 16.6 knots which is above the design speed.

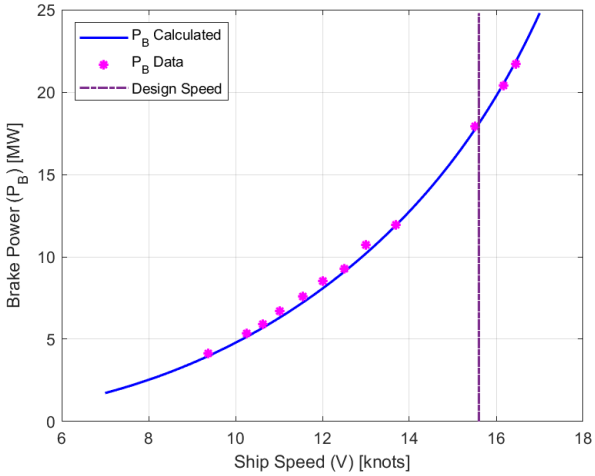

Fig. 28: Engine brake power versus ship speed at trial condition for the example VLCC. Operational data at trial condition is plotted as magenta stars. A numerical comparison of this data is provided in Table VIII.

presents the engine load diagram with calculated propeller curves and trial data denoted. Note that highest log data point occurs at 110% of engine load, and therefore falls outside the operating polygon, as it should. The test data is appropriately bracketed by the propeller curves for trial and heavy running conditions.

Specific fuel oil consumption for the engine tuned to SMCR and for various engine modifications is plotted in Figure 32. From the test data plotted in the figure, it appears that the engine is tuned for lower engine loads, most likely using the ECT low-load modification. Change in fuel oil consumption

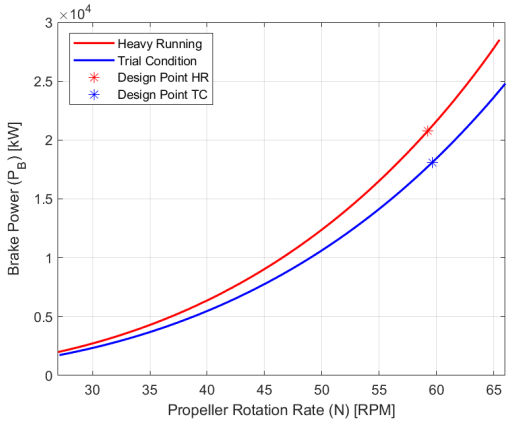

Fig. 29: Engine brake power versus propeller rotation rate for the example VLCC.

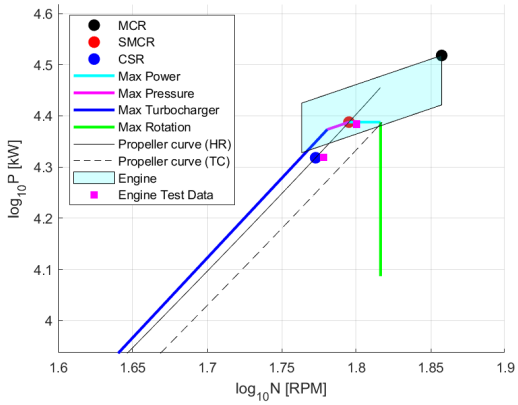

Fig. 30: Log-log plot of the engine load diagram for the example VLCC with calculated and data values for SMCR and CSR denoted.

from the baseline engine tuned to SMCR is shown in Figure 33. Fuel oil consumption in tonnes/day is plotted versus speed for trial condition and heavy running in Figure 34.

B. Product Tanker

The next example is a product tanker. Figures 35 and 36 display the resistance and brake power estimates respectively. The brake power estimate is quite good (less than 3% difference) for the regime dominated by frictional resistance, but begins to diverge a bit as the wave resistance regime is entered, reaching 9.6% difference at 15 knots, where the bulbous bow impacts resistance. This is above the design speed. See Table IX for pertinent data.

We next investigate the impact of various modifications to the ship. Using the baseline data entered for any ship as shown in Table VII, the program generates estimates for the baseline ship, possible engine modifications, ballast condition, and bulb

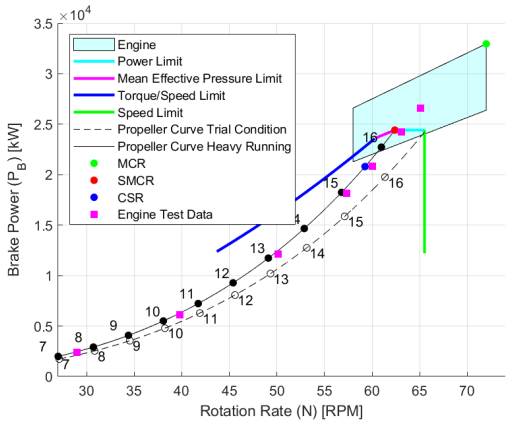

Fig. 31: Engine load diagram for the example VLCC with calculated propeller curves and trial data denoted. Note that highest log data point occurs at 110% of engine load, and therefore should fall outside the operating polygon, as it does.

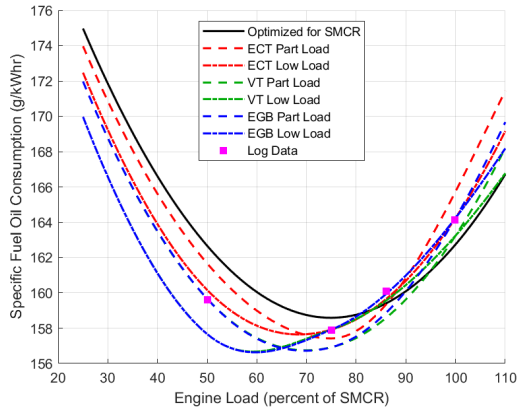

Fig. 32: Specific fuel oil consumption for various engine modifications for the example VLCC along with engine test data.

TABLE IX: Comparison of sea trial data and estimated data for product tanker brake power in MW as plotted in Figure 36.

Speed	Estimate	Log Data	% Difference
11	2.465	2.500	-1.4
12	3.223	3.200	0.7
13	4.187	4.100	2.1
14	5.445	5.250	3.7
15	7.123	6.500	9.6
16	9.403	8.050	16.8

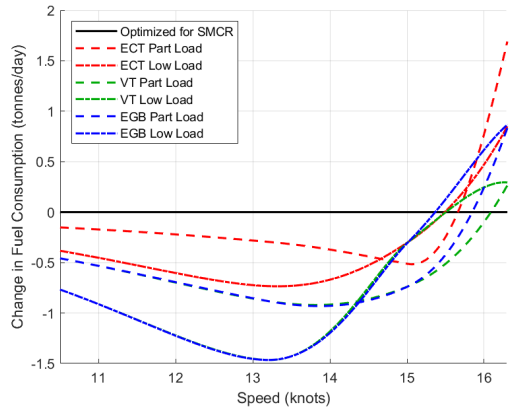

Fig. 33: Change in fuel oil consumption in tonnes/day for various engine modifications for the example VLCC.

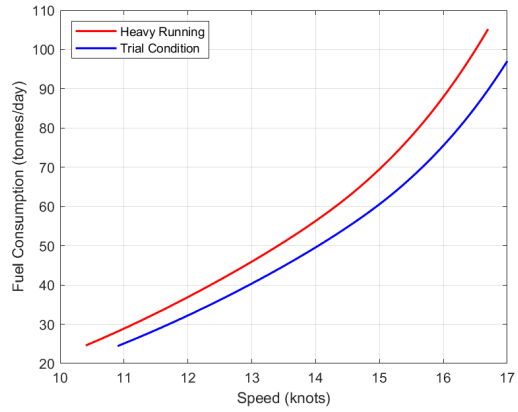

Fig. 34: Fuel oil consumption for the example VLCC as a function of speed for heavy running and trial condition.

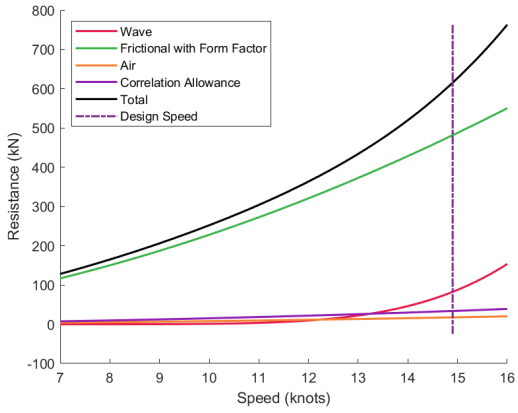

Fig. 35: Resistance calculation results for the example product tanker.

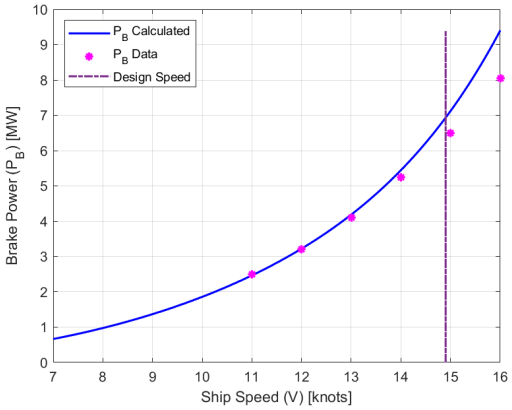

Fig. 36: Engine brake power as a function of ship speed for the example product tanker. Note that the estimate is very close to sea trial data through design speed, but begins to diverge at higher speeds where the bulbous bow estimate is less reliable. See Table IX for a numerical comparison.

TABLE X: Changes to input data for additional runs on example product tanker.

Run	Original Input	Add Mewis Duct	Design Propeller	Mewis and Propeller
energy-saving device	no	yes	no	yes
design speed (knots)	14.9	14.9	12	12
expanded area ratio	0.5411	0.5411	–	–
pitch/ diameter ratio at 0.7R	0.6778	0.6778	–	–

removal if a bulb is present. In order to estimate the impact of an energy-saving device, a separate run is conducted with the ESD flag toggled to "yes." In order to estimate the impact of a new propeller design, a separate run is conducted with the propeller specifications for expanded area ratio and pitch to diameter ratio removed from the input, and a new design speed entered. If a maximum speed above the design speed is desired, that value must be entered as well in order to raise the cavitation limit appropriately. The changes to the product tanker input data to calculate the impact of all these modifications is summarized in Table X.

Figures 37, 38, and 39 show the change in fuel consumption in tonnes/day for the example product tanker for each of several possible modifications. Figure 37 shows modifications to the ship structure, and Figure 38 shows engine modifications. While the engine modifications cannot be combined with each other, any one of them can be combined with the hullform or propeller modifications, and the hullform and propeller modifications can in general be combined with one another. Their effect is not linearly additive, as seen in Figure 39 and Table XI. Note that the new propeller is designed for a speed of 12 knots, and hits a cavitation limit above 13 knots, so is not operated above 13 knots.

TABLE XI: Change in fuel consumption in tonnes/day for various modifications and combinations of modifications to the example product tanker.

Speed	VT Low Load	New Propeller	Mewis Duct	Mewis and VT	Mewis and New Prop	Mewis, Prop and VT
10.5	-0.3	-0.3	-0.7	-0.9	-0.9	-1.2
11	-0.3	-0.4	-0.8	-1.1	-1	-1.4
11.5	-0.4	-0.5	-0.9	-1.3	-1.3	-1.6
12	-0.4	-0.6	-1	-1.5	-1.4	-1.8
12.5	-0.5	-0.6	-1.2	-1.6	-1.6	-2.1
13	-0.5	-0.6	-1.4	-1.9	-1.8	-2.3
13.5	-0.7	–	-1.7	-2.3	–	–
14	-0.4	–	-1.9	-2.3	–	–
14.5	0	–	-2.2	-2.2	–	–
15	0.1	–	-2.6	-2.5	–	–
15.5	0.1	–	-3	-2.9	–	–

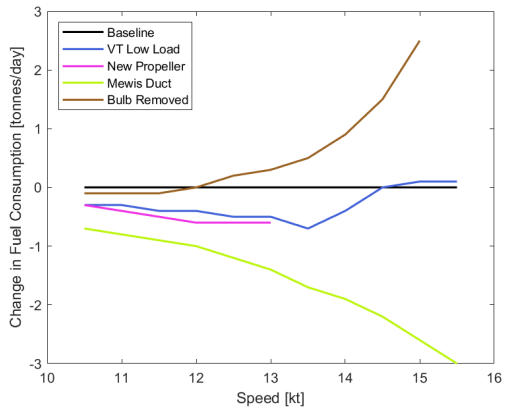

Fig. 37: Change in fuel consumption due to various possible modifications to the example product tanker.

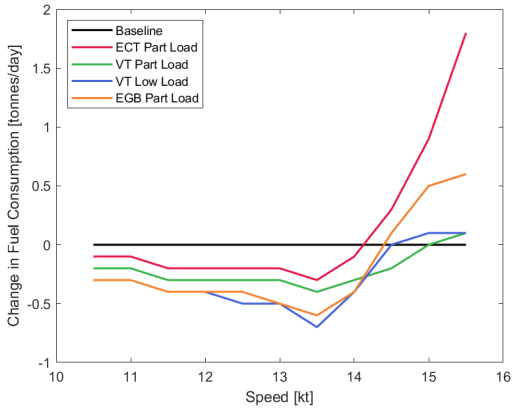

Fig. 38: Change in fuel consumption due to various possible modifications to the engine in the example product tanker.

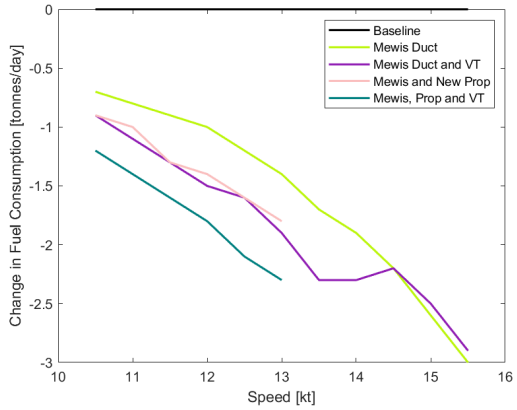

Fig. 39: Combinations of possible modifications to the example product tanker.

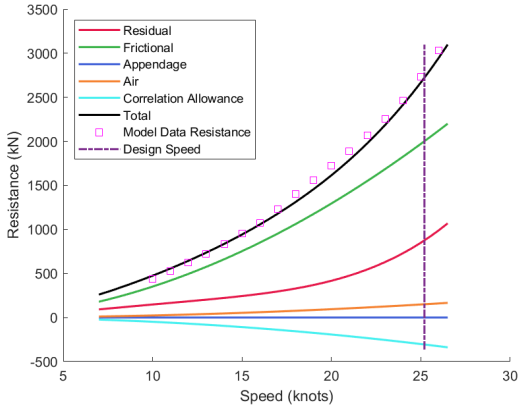

Fig. 40: Resistance calculation results for the example container ship.

C. Container Ship

The final example is a container ship. Container ships typically operate at higher speeds than tankers and thus operate in a regime that includes wave resistance; this can be seen in Figure 40, where wave resistance begins to become significant at about 20 knots. The estimated resistance has quite good correlation with the model test data in this figure, ranging from 0.1 to 6.7 percent difference at any point, even extending into the wave resistance regime. The close correlation is especially notable in view of the uncertainty involved in estimating the impact of the bulbous bow.

Another area of interest in this example is the propeller curves. Container ships tend to have more complex propellers with greater skew and rake than a tanker propeller, so there was some concern that using the Wageningen B-Series as an estimate of propeller performance might be a source of error; however, we find good correlation between the estimated propeller and propeller test data provided by the ship owner.

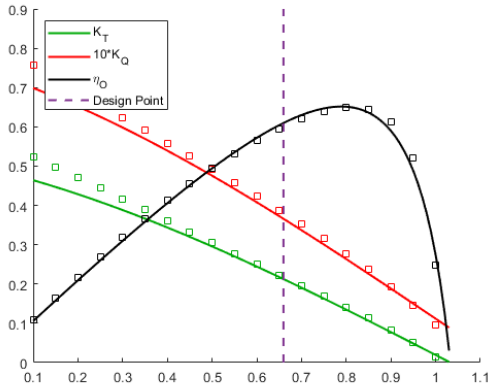

Fig. 41: Propeller curves for the example container ship.

In Figure 41, the calculated propeller data is shown using solid lines and the corresponding actual propeller data is plotted using squares. In the operational regime for this vessel, J is between 0.64 and 0.685, and the calculated propeller efficiencies in this range are within 2% of the actual values, as shown in Table XII.

TABLE XII: Comparison of log data and estimated data for container ship propeller curves.

Advance Ratio J	0.60	0.65	0.70
K_T Calculated	0.244	0.218	0.191
K_T Data	0.251	0.223	0.196
K_T % Difference	2.7	2.4	2.8
K_Q Calculated	0.408	0.373	0.337
K_Q Data	0.423	0.388	0.353
K_Q % Difference	3.6	3.9	4.6
η_o Calculated	0.572	0.604	0.630
η_o Data	0.565	0.595	0.620
η_o % Difference	1.2	1.5	1.6

The resulting speed-power curve, shown in Figure 42, has quite close correlation with model test data, showing a maximum of 6.7 percent difference through the entire speed range, even in the wave-dominated regime, as shown in Table XIII.

This ship employs a Wärtsilä engine, so a different array of tuning technologies are available than for the MAN B&W engines used by the previous two example vessels. The impacts of these technologies on fuel consumption for this example ship are shown in Figure 43.

D. Example Summary

We have presented example calculations for three types of ships: a container ship, a product tanker, and a VLCC. These examples thoroughly demonstrate the capabilities of the code. Further, the comparison of each ship to operational or test data shows exceptional correlation between the program's calculations and actual ship data, especially given the simplicity of the inputs provided.

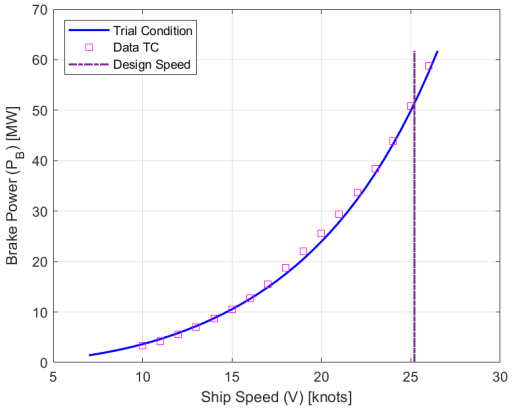

Fig. 42: Speed versus power curve for the example container ship.

TABLE XIII: Comparison of log data to estimated data for container ship total resistance.

Speed	Estimate	Log Data	% Difference
12	5,550	5,840	5.2
13	6,994	7,206	3.0
14	8,664	8,771	1.2
15	10,576	10,557	-0.2
16	12,749	12,591	-1.2
17	15,524	14,906	-4.0
18	18,712	17,541	-6.3
19	22,029	20,542	-6.7
20	25,555	23,964	-6.2
21	29,435	27,867	-5.3
22	33,684	32,325	-4.0
23	38,381	37,422	-2.5
24	43,847	43,251	-1.4
25	50,778	49,922	-1.7
26	58,757	57,558	-2.0

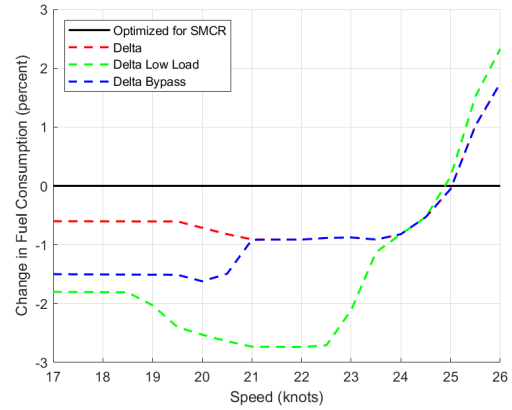

Fig. 43: Change in fuel oil consumption for various engine modifications for the container ship.

XII. User's Manual

This section provides instructions on the use of the program including input data, running the program, modifying default values, and output data.

A. Input Data

Ship data is input via an excel spreadsheet, and is divided into four tabs: hull, engine, prop and conditions. There is a minimum set of mandatory data, without which the program cannot run. The remainder of the data is optional; however, the more data that is input, the more accurate the estimates of performance will be. It is extremely important that data is self-consistent; *e.g.*, draft, displacement and wetted surface area must all correspond to the same draft value. Data descriptions can be found in Tables XIV through XVII. The minimum input data required is summarized in Table XVIII.

B. Basic Program Setup and Running

The program is started in Matlab by running `AA0_StartHere.m`. Prior to running, a few steps should be checked:

a) Folder Setup: First, ensure that there is a folder named "RESULTS" in the active directory, and within the RESULTS folder, there is a folder named "FIGS". Output will be placed in these folders.

b) Plotting Flag: Within the `AA0_StartHere.m` file, line 12 has a plotting flag, named "constants.yesPlot". If yesPlot is equal to zero, no plots will be created. Setting yesPlot equal to two yields verbose mode with 20 plots presented, and setting yesPlot equal to one yields nine plots.

c) Input Data: The program takes input from two files: `input.xlsx` and `engineData.xlsx`. The user should place ship data in each tab of `input.xlsx` and ensure that the ship name is consistent on each of the four tabs in the input file.

An engine library containing data on a wide range of engines is provided with the program. The user should ensure that the engine model placed on the engine tab of `inputs.xlsx` matches the model name of one of the engines in `engineData.xlsx`. It is possible to add new engines to the engineData library if needed. Two formats are provided; either entry on a single line in the first tab of the spreadsheet, or entry as a full page of data in its own tab. Example sheets are provided for copying.

C. Advanced Program Modifications

Within the `AA0_StartHere.m` file, line 10 contains the input file name; it is set to "inputs.xlsx", but can be changed by the user.

Several limits are set within `INPUT_Data.m`. While we have selected values appropriate to most applications, and do not recommend changing these limits, it is possible for the user to modify these values in the code prior to running. Specific limits follow; all are values in the struct "constant".

- *lowspeed* is the lowest speed that is calculated by the program. This is set to 7 knots.

TABLE XIV: Hull Data, entered on the "hull" tab of `inputs.xlsx`

Abbr	Name	Required?	Units or Enumeration	Description
Flags				
	Ship Type	yes	enumeration	Class or type of ship, enumeration choices: tanker / container / bulker
	Bulbous Bow Flag	yes	yes / no	Indicates whether a bulbous bow is present
	Energy Saving Device	yes	yes / no	Indicates whether a Mewis duct is installed
Hull Data				
	Design Speed	yes	[knots]	The design speed
L_{bp}	Length Between Perpendiculars			
L_{wl}	Length at Waterline	yes	[m]	Some indication of length is required. The preference is for both L_{bp} and L_{wl} to be provided, but any one of L_{bp}, L_{wl} or L_{oa} will suffice.
L_{oa}	Length Overall			
B	Beam	yes	[m]	Extreme breadth at waterline
Data at Design Draft				
T_f	Draft Forward	yes	[m]	Design draft at the forward perpendicular
T_a	Draft Aft	yes	[m]	Design draft at the aft perpendicular
Δ	Displacement	yes	[tonnes]	Displacement at design draft. Either Displacement or DWT must be provided; displacement is preferred.
DWT	Deadweight			
lcb_{ap}	Longitudinal Center of Buoyancy		[m]	Distance from longitudinal center of buoyancy to the aft perpendicular
A_{ws}	Wetted Surface Area		[m^2]	Area of the bare hull at design draft
A_{exp}	Area exposed to wind		[m^2]	Athwartships cross-sectional area above the waterline, orthogonal to the direction of travel
d_{ap}	AP to aftmost point		[m]	Distance from aft perpendicular to aftmost point of wet hull at design draft
Data at Ballast Draft				
T_{fB}	Draft Forward	see note	[m]	Draft at the forward perpendicular in ballast condition
T_{aB}	Draft Aft	see note	[m]	Draft at the aft perpendicular in ballast condition
Δ_B	Displacement		[tonnes]	Displacement at ballast draft
lcb_B	Longitudinal Center of Buoyancy		[m]	Distance from longitudinal center of buoyancy at ballast to the aft perpendicular
A_{wsB}	Wetted Surface Area		[m^2]	Area of the bare hull at ballast
A_{expB}	Cross-sectional Area		[m^2]	Athwartships cross-sectional area above the waterline, orthogonal to direction of travel, at ballast
Note: if ballast condition is to be calculated, ballast draft forward and aft must be provided				
Hullform Coefficients				
C_x	Midship Section Coefficient		non-dimensional	Area of the midship section divided by beam times draft, at design draft
C_{wp}	Waterplane Coefficient		non-dimensional	Area of waterplane divided by length times beam, at design draft
Bulbous Bow Data				
L_b	Bulb Length		[m]	Length of bulb extent forward of forward perpendicular
A_{bt}	Bulb Transverse Area		[m^2]	Transverse sectional area of bulb where still water surface intersects the stem
h_b	Vertical Centroid of A_{bt}		[m]	Vertical centroid of bulb transverse sectional area above baseline
A_b	Bulb Surface Area		[m^2]	Wetted surface area of the bulb
∇_b	Bulb Volume		[m^3]	Volume of the bulb
Appendage Wetted Surface Area				
A_{app_i}	Appendage Wetted Surface Area		[m^2]	Wetted surface area of various appendages

TABLE XV: Engine Data, entered on the "engine" tab

Name	Required?	Description
Engine Make		Make of the engine, MAN, Wärtsilä or other
Engine Model	yes	Engine model. Must match data in engine library
Engine Control	yes	Engine control methodology, 'camshaft' or 'electronic'
Number of Cylinders	yes	Number of cylinders in engine
Number of Turbochargers		Number of turbochargers

TABLE XVI: Propeller Data, entered on the "prop" tab

Abbr	Name	Required?	Units	Description
N_p	Number of Propellers	yes		Number of propellers
D	Diameter		[m]	Diameter of the propeller
h_z	Propeller Height		[m]	Height of the center of the propeller above the baseline
Z	Number of Blades			Number of blades on each propeller
AE/AO	Expanded Area Ratio		non-dimensional	Propeller blade expanded area divided by the area of the propeller disk
P/D	Pitch to Diameter Ratio		non-dimensional	Propeller pitch at 0.7 radius, divided by propeller diameter

TABLE XVII: Conditions and Margin Data, entered on the "conditions" tab

Name	Required?	Default Value	Description
Engine Margin		10%	Percent increase in propulsion power for engine design point calculations
Sea Margin		15%	Percent increase in propulsion power due to high sea state
Shaft Efficiency		99%	Transmission efficiency between engine and propeller
Propeller Margin		5%	Percent decrease in propeller rotation rate used for engine design point calculations

TABLE XVIII: Minimum Required Input Data

Displacement or Deadweight
Length
Beam
Draft
Design Speed
Number of Propellers
Ship Type Indicator (Tanker, Container)
Bulbous Bow Indicator (yes, no)
ESD Indicator (yes, no)
Engine Layout Diagram including for each corner:
Rotation Rate
Brake Power
Mean Effective Pressure
Specific Fuel Oil Consumption

- *percentloadmin* is the minimum engine load for which fuel consumption is calculated, set to 25%.
- *percentloadmax* is the maximum engine load for which fuel consumption is calculated, set to 110%.
- *wmin* is the minimum value that the wake fraction, w, is allowed to take, set to 0.1.
- *wmax* is the maximum value that the wake fraction, w, is allowed to take, set to 0.5.
- *tmin* is the minimum value that the thrust deduction factor, t, is allowed to take, set to 0.1.
- *tmax* is the maximum value that the thrust deduction factor, t, is allowed to take, set to 0.25.
- *etarmin* is the minimum value that the relative rotative efficiency, η_r, is allowed to take, set to 0.95.
- *etarmax* is the maximum value that the relative rotative efficiency, η_r, is allowed to take, set to 1.05.

D. Numerical Output

Each time it is run, the program places a time-stamped output file in "../RESULTS". In this excel file, there will be a separate tab for each ship and each condition. For example, if the input data contains a ship named "thisShip", output tabs will be named "thisShip", "thisShip BALLAST", "thisShip NO BULB", and "thisShip BALLAST NO BULB", assuming that input contains ballast data and that the ship has a bulbous bow that is removed.

Each tab contains in the first three columns a tabulation of input data. The first column contains the variable name, the second column contains data values input by the user and the third column contains data values used by the program, thus providing the user any values that were estimated by the program. As an example, in the screenshot shown in Figure 44, note that the user did not input values for the expanded-area ratio or the pitch-to-diameter ratio of the propeller, so the program calculated them; thus, column B reads zero for each value whereas column C reads 0.371 and 0.77 respectively.

	A	B	C	D
1	thisShip	Input Val	Calc Val	
29				
30	Propeller Data			
31				
32	Propeller Diameter	9.9	9.9	
33	Number of Blades	4	4	
34	Expanded Area Ratio	0	0.371	
35	Pitch to Diameter Ratio	0	0.77	
36				
37	Engine Data			
38				
39	Engine	Wartsila	G80ME-C9-2	
40	Number of Cylinders	7		
41	Number of Turbochargers			
42				

Fig. 44: Output File listing of data input (column B) and data used (column C).

Each page tabulates the resistance, effective power, and

brake power for trial condition and heavy running over a full range of speeds. Specific fuel oil consumption (SFOC) and fuel oil consumption (FOC) for the engine tuned to SMCR are provided for speeds corresponding to a range of 25-110% engine power; see Figure 45. Next, FOC and SFOC for the heavy running case with each applicable engine modification are tabulated as shown in Figure 46. Farther to the right in the output file, details of the propeller calculations and the resistance calculations are tabulated as shown in Figures 47 and 48 respectively.

thisShip						
Speed (kt)	Resistance (kN)	Effective Power (kW)	Brake Power TC (kW)	Brake Power HR (kW)	SFOC HR at SMCR (g/kWhr)	FOC HR at SMCR (tonnes/day)
7	358.3	1290.2	1862.5	2141.8		
7.5	407.5	1572.3	2265.7	2605.5		
8	459.7	1891.7	2721.7	3129.9		
8.5	514.7	2250.7	3233.5	3718.6		
9	572.7	2651.5	3804.2	4374.9		
9.5	633.5	3096.3	4436.8	5102.3		
10	697.3	3587.3	5134.5	5904.7		
10.5	764	4126.8	5900.6	6785.7	166	27
11	833.7	4717.6	6738.9	7749.7	166	30.9
11.5	906.4	5362.5	7653.7	8801.8	165.7	35
12	982.4	6064.9	8650.3	9947.8	164.9	39.4
12.5	1062	6829.1	9735.1	11195.4	163.7	44
13	1145.4	7660.2	10916.3	12553.7	162.1	48.9
13.5	1233.2	8564.8	12204.4	14035.1	160.3	54
14	1326.1	9550.9	13612.9	15654.9	158.6	59.6
14.5	1424.9	10629	15158.9	17432.8	157.3	65.8
15	1530.7	11811.9	16864.1	19393.7	157.1	73.1
15.5	1644.8	13115.4	18755.5	21568.8	157.7	81.7
16	1768.8	14559	20866.8	23996.9	159.3	91.8
16.5	1904.5	16166.1	23239.4	26725.3	161.7	103.7
17	2054.1	17964.5	25923.6	29812.1		
17.5	2220.1	19987	28980.2	33327.2		
18	2405.2	22271.8	32482.2	37354.5		
18.5	2612.4	24863.1	36517	41994.5		
19	2845.3	27810.9	41188.4	47366.7		

Fig. 45: Output File tabulation of resistance, power, SFOC and FOC at SMCR.

thisShip	Fuel Oil Consumption, Heavy Running (tonnes/day)							Specific Fuel Oil Consumption, Heavy Running (g/kWhr)						
Speed (kt)	at SMCR	ECT Part Load	ECT Low Load	VT Part Load	VT Low Load	EGB Part Load	EGB Low Load	at SMCR	ECT Part Load	ECT Low Load	VT Part Load	VT Low Load	EGB Part Load	EGB Low Load
7														
7.5														
8														
8.5														
9														
9.5														
10														
10.5	27	26.9	26.6	26.5	26.2	26.5	26.2	166	165	163.5	163	161	163	161
11	30.9	30.7	30.4	30.3	29.9	30.3	29.9	166	165	163.4	162.9	160.7	162.9	160.7
11.5	35	34.8	34.4	34.3	33.9	34.3	33.9	165.7	164.7	163	162.6	160.3	162.6	160.3
12	39.4	39.1	38.7	38.6	38.1	38.6	38.1	164.9	163.9	162.2	161.8	159.4	161.8	159.4
12.5	44	43.7	43.3	43.2	42.5	43.2	42.5	163.7	162.7	161	160.6	158.3	160.6	158.3
13	48.9	48.6	48.1	47.9	47.3	47.9	47.3	162.1	161.1	159.6	159.1	157	159.1	157
13.5	54	53.7	53.2	53	52.5	53	52.5	160.3	159.3	158	157.5	155.8	157.4	155.8
14	59.6	59.2	58.9	58.6	58.3	58.6	58.3	158.6	157.5	156.7	156	155.2	156	155.2
14.5	65.8	65.4	65.3	64.9	65	64.9	65	157.3	156.2	156	155.1	155.4	155.1	155.3
15	73.1	72.6	72.8	72.3	72.8	72.3	72.8	157.1	155.9	156.3	155.4	156.3	155.4	156.3
15.5	81.7	81.3	81.6	81.1	81.6	81.2	81.8	157.7	157.2	157.7	156.6	157.7	156.8	157.9
16	91.8	92.4	92.2	91.6	92	91.9	92.4	159.3	160.5	160.1	159	159.7	159.6	160.4
16.5	103.7	105.9	104.8	104.2	104	104.9	104.7	161.7	165.2	163.4	162.4	162.1	163.5	163.2
17														
17.5														
18														
18.5														
19														

Fig. 46: Output File tabulation of FOC and SFOC.

E. Graphical Output

Graphical output includes the following plots, examples of which can be found throughout this report.

- Resistance (Figure 1)
- Propeller design points for various pitch to diameter ratios (Figure 16)
- Propeller selection plotted on engine diagram (Figure 17)
- Engine operating point (Figure 18)

Propeller Data								
Ship Speed (kt)	Thrust Deduction	Wake Fraction	Hull Efficiency	Propeller Open Water	Relative Rotative	Shaft Efficiency	Mewis efficiency	Total Efficiency
7	0.218	0.3922	1.2865	0.5393	1.0242	0.975	1	0.6928
7.5	0.218	0.3915	1.2852	0.5408	1.0242	0.975	1	0.694
8	0.218	0.3909	1.2839	0.5421	1.0242	0.975	1	0.6951
8.5	0.218	0.3904	1.2828	0.5434	1.0242	0.975	1	0.6961
9	0.218	0.3899	1.2817	0.5446	1.0242	0.975	1	0.697
9.5	0.218	0.3894	1.2807	0.5457	1.0242	0.975	1	0.6979
10	0.218	0.389	1.2798	0.5467	1.0242	0.975	1	0.6987
10.5	0.218	0.3885	1.2789	0.5476	1.0242	0.975	1	0.6994
11	0.218	0.3882	1.2781	0.5485	1.0242	0.975	1	0.7001
11.5	0.218	0.3878	1.2773	0.5493	1.0242	0.975	1	0.7006
12	0.218	0.3874	1.2766	0.55	1.0242	0.975	1	0.7011
12.5	0.218	0.3871	1.2759	0.5506	1.0242	0.975	1	0.7015
13	0.218	0.3868	1.2752	0.5511	1.0242	0.975	1	0.7017
13.5	0.218	0.3865	1.2746	0.5514	1.0242	0.975	1	0.7018
14	0.218	0.3862	1.274	0.5515	1.0242	0.975	1	0.7016
14.5	0.218	0.3859	1.2734	0.5514	1.0242	0.975	1	0.7012
15	0.218	0.3856	1.2729	0.5511	1.0242	0.975	1	0.7004
15.5	0.218	0.3854	1.2723	0.5504	1.0242	0.975	1	0.6993
16	0.218	0.3851	1.2718	0.5494	1.0242	0.975	1	0.6977
16.5	0.218	0.3849	1.2713	0.5479	1.0242	0.975	1	0.6956
17	0.218	0.3847	1.2709	0.5461	1.0242	0.975	1	0.693
17.5	0.218	0.3845	1.2704	0.5437	1.0242	0.975	1	0.6897
18	0.218	0.3842	1.27	0.5407	1.0242	0.975	1	0.6857
18.5	0.218	0.384	1.2696	0.5371	1.0242	0.975	1	0.6809
19	0.218	0.3838	1.2692	0.5328	1.0242	0.975	1	0.6752

Fig. 47: Output File tabulation of propeller calculations.

Holtrop & Mennen Resistance Results								
speed	frictional	form factor	frictional* form factor	appendage	wave	air	correlation allowance	total
7	291.9	1.3	387.3	1.7	0.0	7.8	-38.5	358.3
7.5	332.3	1.3	440.8	2.0	0.0	9.0	-44.2	407.5
8	375.1	1.3	497.5	2.2	0.0	10.2	-50.3	459.7
8.5	420.3	1.3	557.5	2.5	0.0	11.5	-56.8	514.7
9	467.9	1.3	620.7	2.8	0.0	12.9	-63.7	572.7
9.5	517.9	1.3	687.0	3.1	0.1	14.4	-70.9	633.5
10	570.3	1.3	756.5	3.4	0.1	15.9	-78.6	697.3
10.5	625.0	1.3	829.1	3.7	0.3	17.5	-86.7	764.0
11	682.1	1.3	904.8	4.1	0.6	19.3	-95.1	833.7
11.5	741.5	1.3	983.7	4.4	1.3	21.0	-104.0	906.4
12	803.3	1.3	1065.6	4.8	2.4	22.9	-113.2	982.4
12.5	867.4	1.3	1150.6	5.2	4.2	24.9	-122.8	1062.0
13	933.7	1.3	1238.6	5.5	7.2	26.9	-132.8	1145.4
13.5	1002.4	1.3	1329.7	6.0	11.8	29.0	-143.3	1233.2
14	1073.4	1.3	1423.9	6.4	18.7	31.2	-154.1	1326.1
14.5	1146.6	1.3	1521.0	6.8	28.9	33.5	-165.3	1424.9
15	1222.1	1.3	1621.2	7.3	43.3	35.8	-176.9	1530.7
15.5	1299.9	1.3	1724.4	7.7	63.3	38.2	-188.9	1644.8
16	1379.9	1.3	1830.5	8.2	90.6	40.7	-201.2	1768.8
16.5	1462.2	1.3	1939.7	8.7	126.8	43.3	-214.0	1904.5
17	1546.7	1.3	2051.8	9.2	174.4	46.0	-227.2	2054.1
17.5	1633.5	1.3	2166.8	9.7	235.5	48.7	-240.7	2220.1
18	1722.4	1.3	2284.9	10.2	313.2	51.6	-254.7	2405.2
18.5	1813.6	1.3	2405.8	10.8	410.4	54.5	-269.0	2612.4
19	1907.0	1.3	2529.7	11.3	530.6	57.4	-283.8	2845.3

Fig. 48: Output File tabulation of resistance calculations.

- Brake power vs. ship speed (Figure 28)
- Propeller input data (Figure 23)
- Propeller curves and operating point (Figure 25)
- Propeller rotation rate vs. ship speed (Figure 5 center)
- Engine brake power vs. propeller rotation rate
- Propeller efficiency vs. ship speed (Figure 5 right)
- Engine load diagram, log-log plot (Figure 30)
- Engine load diagram with propeller curves and engine operating polygon (Figure 10)
- Cavitation limit as a function of cavitation number (Figure 7 top)
- Cavitation limit vs. ship speed (Figure 7 bottom)
- Daily fuel consumption vs. percent engine load, heavy running, for various tuning technologies
- Specific fuel oil consumption vs. ship speed for heavy running and various tuning technologies (Figure 32)

- Change in daily fuel consumption in tonnes/day vs. ship speed (Figure 33)
- Percent change in daily fuel consumption vs. ship speed
- SFOC for various tuning technologies vs. percent engine load
- Daily fuel consumption vs. speed, optimized for SMCR, heavy running and trial conditions (Figure 34)

XIII. Conclusions and Future Work

The goal of this project is to reduce carbon production of the existing cargo shipping fleet by providing an easy-to-use tool that assesses the impact that various fuel-saving methods and technologies have on fuel consumption. The code uses a small set of input data to estimate baseline ship performance and then provides the energy-saving impact of slow steaming, propeller redesign, bulbous bow removal, engine modifications, and energy-saving device installation.

The code is written in Matlab and is available online at https://seagrant.mit.edu/decarbonization.

The code is applicable to direct-drive ships with fixed-pitch propellers and with no reduction gear. Possible future expansions that would be relatively simple to implement would be to improve twin-screw estimates and add capability for reduction gears, controllable-pitch propellers, and electric drive or power-take-off configurations.

Additional energy saving devices beyond the Mewis Duct warrant further investigation as well.

There are a number of quite interesting energy-saving methods that are not examined in the current project such as waste-heat recovery, energy storage, air lubrication of the hull, or incorporation of renewable resources such as wind power. These would likely require significant modification to existing ships, but have the potential to provide significant energy savings.

Machine-learning techniques and the use of big data would be useful to parse voyage data for prediction of maintenance and repair needs which can unearth energy-saving methods such as timely hull cleaning with low cost and high impact.

Acknowledgements

The authors would like to thank the following people for their excellent contributions and interesting discussions.

Prof. Pradya Prempraneerach was involved in the beginning of the project but, because of travel restrictions due to the pandemic, was unable to continue the collaboration. His original contributions were extremely valuable.

Hauke Kite-Powell of Marsoft, Inc., used the code extensively, providing testing and feedback on all features. His testing has greatly improved the robustness of the code.

Lily Keyes conceptualized and implemented the cover art.

References

[1] Lothar Birk. *Fundamentals of Ship Hydrodynamics: Fluid Mechanics, Ship Resistance and Propulsion*. John Wiley & Sons Ltd, Hoboken, NJ, USA, first edition, 2019.

[2] Scott D. Black. Thrust breakdown characteristics of conventional propellers. Technical Report NSWCCD-50-TR-2007/064, Naval Surface Warfare Center Carderock Division, September 2007.

[3] Luca Bonfiglio and Dario Boote. Progetto di massima di una portacontenitori da 9000 teu. Master's thesis, Università di Genova, 2009.

[4] Ø Buhaug, JJ Corbett, O Endresen, V Eyring, J Faber, S Hanayama, D Lee, H Lindstad, A Mjelde, C Palsson, et al. Second IMO greenhouse gas study. *International Maritime Organization, London*, 2009.

[5] John Carlton. *Marine propellers and propulsion*. Butterworth-Heinemann, 2018.

[6] R. W. Gawn and L. C. Burrill. Effect of cavitation on the performance of a series of 16 inch model propellers. *Royal Institute of Naval Architects*, 1957.

[7] Thomas Guiard, Steven Leonard, and Friedrich Mewis. The Becker Mewis Duct® - challenges in full-scale design and new developments for fast ships. In *Third International Symposium on Marine Propulsors (SMP'13)*, Launceston, Tasmania, Australia, May 2013.

[8] HE Guldhammer and Sv Aa Harvald. Ship resistance - effect of form and principal dimensions (revised). *Danish Technical Press, Danmark, Danmarks Tekniske Hojskole, kademisk Forlag, St. kannikestrade 8, DK 1169 Copenhagen*, 1974.

[9] J. Holtrop. Statistical re-analysis of resistance and propulsion data. *International Shipbuilding Progress*, 31(363):272–276, 1984.

[10] J. Holtrop. A statistical resistance prediction method with a speed dependent form factor. In *Proceedings of SMSSH (Scientific and Methodological Seminar on Ship Hydrodynamics)*, pages 1–7, Varna, Bulgaria, October 17-22 1988.

[11] J. Holtrop and G. G. J. Mennen. A statistical power prediction method. *International Shipbuilding Progress*, 25(290):253–256, 1978.

[12] J. Holtrop and G. G. J. Mennen. An approximate power prediction method. *International Shipbuilding Progress*, 29(335):166–170, 1982.

[13] Alfred M Kracht. Design of bulbous bows. *SNAME Transactions*, 86(1):197–217, 1978.

[14] Hans Otto Kristensen and Marie Lützen. Prediction of resistance and propulsion power of ships. *Clean Shipping Currents*, 1(6):1–52, 2012.

[15] E.V. Lewis, editor. *Principles of Naval Architecture*, volume II. Society of Naval Architects and Marine Engineers, Jersey City, NJ, USA, second edition, 1988. Volume II – Resistance, Propulsion and Vibration.

[16] MAN Diesel & Turbo. Basic principles of ship propulsion. Technical report, MAN Diesel & Turbo, 2011.

[17] Friedrich Mewis and Thomas Guiard. Mewis duct – new developments, solutions and conclusions. In *Second International Symposium on Marine Propulsors (SMP'11)*, Hamburg, Germany, June 2011.

[18] Anthony F Molland, Stephen R Turnock, and Dominic A Hudson. *Ship resistance and propulsion*. Cambridge university press, 2017.

[19] National Oceanic and Atmospheric Administration. Ocean acidification, 2020. https://www.noaa.gov/education/resource-collections/ocean-coasts/ocean-acidification.

[20] American Bureau of Shipping. Guidance notes on ship vibration. Technical report, American Bureau of Shipping, February 2018.

[21] United Nations Conference on Trade and Development. Review of maritime transport 2018, 2018.

[22] International Maritime Organization. Reducing greenhouse gas emissions from ships, 2020. https://www.imo.org/en/MediaCentre/HotTopics/Pages/Reducing-greenhouse-gas-emissions-from-ships.aspx.

[23] Herbert Schneekluth and Volker Bertram. *Ship design for efficiency and economy*, volume 218. Butterworth-Heinemann Oxford, 1998.

[24] Pieter Tans, Ed Dlugokencky, and Ben Miller. The power of greenhouse gases, October 2020. https://www.esrl.noaa.gov/gmd/ccgg/ghgpower/.

[25] R. L. Thoman, J. Richter-Menge, and M. L. Druckenmiller, editors. *Arctic Report Card 2020*. National Oceanic and Atmospheric Administration, 2020.

[26] David G. M. Watson. *Practical Ship Design*. Elsevier, Kidlington, Oxford, UK, first edition, 2002.

APPENDIX

A. Bulbous Bow Effects

A properly designed bulbous bow reduces propulsion power at and around the designed operating speed of the ship. When a ship is operated at a speed significantly different from the speed for which the bulb was designed, the bulb can have an adverse effect on the resistance of the ship, increasing propulsion power and, thus, fuel consumption. This variation in the impact of the bulbous bow is shown in Figure 19 from Carlton [5], who states that the positive impact of bulbous bows occurs over a narrow range of ship speeds, so they are usually employed in ships that operate at clearly defined speeds for much of their time. If a ship is operated consistently off-design, e.g. due to a new operational profile, it may be cost effective to modify the bulb's shape or to remove the bulb entirely.

The main effect of a bulbous bow is to reduce the ship's bow wave by creating a wave that is out of phase with the bow wave. The bulb also has some less pronounced positive effects due to changing the flow of water past the hull, e.g. reduction of the breaking of the bow wave, changes in the energy in the vortices originating at the bow, and changes in the streamlines at the bow. The change in flow pattern persists to the stern and the propeller, and thus impacts the wake fraction and thrust deduction factor, affecting the propulsive efficiency of the propeller. Kracht [13] provides diagrams of the impact of two specific bulbs on the wake fraction and thrust deduction factor, shown in Figure 49.

The advantages of a bulbous bow are somewhat reduced by an increase in frictional resistance due to the increased surface area of the hull; therefore, at slow speeds where wave resistance is very small relative to frictional resistance, the bulbous bow can increase resistance. Further, at some non-optimum higher speeds, it is possible that the bulbous bow may increase wave resistance if the wave created by the bulb is not out of phase with the ship's bow wave.

It is definitely agreed upon that the impact of the bulbous bow increases with increasing Froude number to a maximum value, then decreases again to zero at very high Froude numbers. The performance of the bulbous bow is different at laden and ballast drafts; the impact is generally greater, i.e. more beneficial, at ballast, especially for ships with large block coefficients.

B. Bulbous Bow Ranges of Applicability

Figure 50 from Watson [26] shows the combinations of Froude number and block coefficient for which a bulb is likely to be advantageous at full load draft. For finer ships, the bulb is advantageous at high speeds, whereas for ships with a high block coefficient, the bulb is advantageous over a wider range of Froude numbers. Although he does not provide an equivalent diagram for a ship operating at ballast, Watson does state that a bulb is advantageous at ballast even if not advantageous when laden *if* the ship operates at full power and thus higher speeds (on the order of two knots greater) at ballast than laden. This advantage at ballast condition is greatest on ships with block coefficients greater than 0.75.

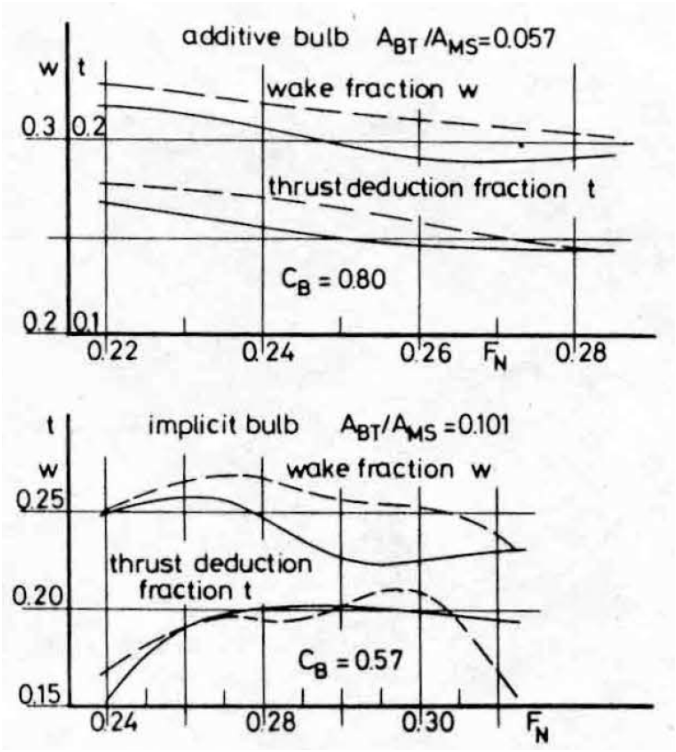

Fig. 49: Change in thrust deduction and wake fraction for two bulbs (dashed lines with bulb, solid lines without bulb) [13]

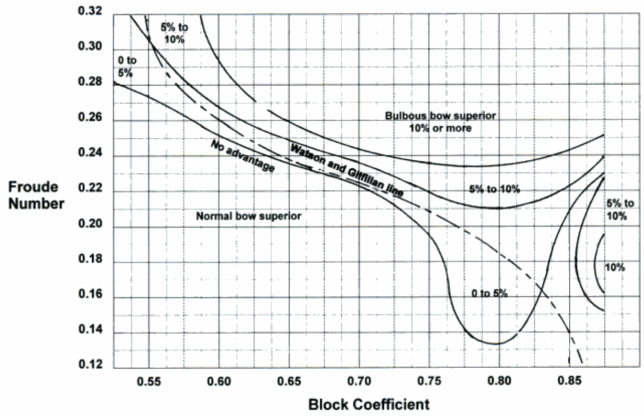

Fig. 50: Areas of advantageous employment of a bulbous bow [26]

Guldhammer and Harvald [8] present a modification to the ship resistance for a bulbous bow which varies with Froude number and block coefficient of the ship and with the transverse cross-sectional area of the bulb at the forward perpendicular relative to the area of the maximum section. The numerical values ($\times 10^3$) of the bulbous bow resistance coefficient are shown in Table XIX. Note the greater impact at higher speeds and lower block coefficients. They further

state that the impact relative to block coefficient is reversed at ballast condition: full forms, with block coefficients greater than 0.70, show a large decrease in resistance with two to three times the values shown in Table XIX, and fine forms, with block coefficients less than 0.6, will tend to increase.

Fn =	0,15	0,18	0,21	0,24	0,27	0,30	0,33	0,36	Φ
			+0,2	0	-0,2	-0,4	-0,4	-0,4	0,50
			+0,2	0	-0,2	-0,3	-0,3		0,60
		+0,2	0	-0,2	-0,3	-0,3			0,70
	+0,1	0	-0,2						0,80

TABLE XIX: Bulbous bow impact coefficient of resistance $\times 10^3$ for fully laden ships as a function of Froude number, Fr, and block coefficient, ϕ, for a bulbous bow with transverse sectional area greater than or equal to ten percent of the ship maximum sectional area [8].

Data on several pertinent ships with bulbous bows is plotted on the chart provided by Watson in Figure 51. It is interesting that several ships with bulbous bows fall within the area of the plot described as not advantageous for bulbous bows. All of these ships are newer than the original plot, which was published in 2002. These same ships are plotted using the resistance coefficients provided by Guldhammer and Harvald in Figure 52, and again we see that several ships fall into the area in which Guldhammer and Harvald predict an increase in resistance at design speed. One must surmise that either the ship designers purposefully created ships with poor performance, or that progression in bulbous bow design has changed the performance of ships with bulbs since Watson, Guldhammer and Harvald made their assessments.

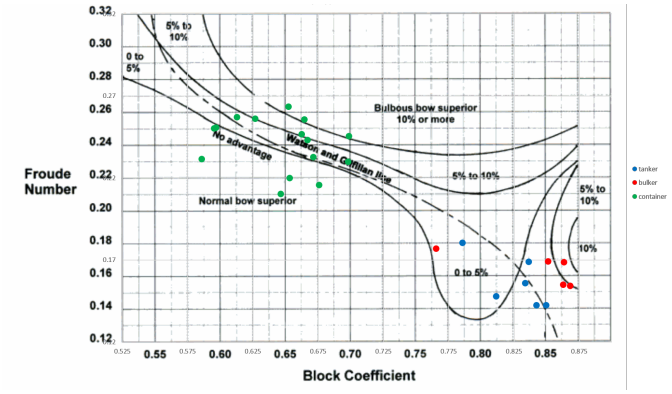

Fig. 51: Ship data for new ships with bulbs plotted against recommendations from [26]. Green dots are container ships, red dots are bulkers, and blue dots are tankers.

C. Methods of Estimating Bulbous Bow Effect

a) Schneekluth and Bertram: Schneekluth and Bertram [23] provide a thorough description of the methodology by which a bulbous bow reduces ship resistance. They describe the estimation of the impact of a bulbous bow by using a power-equivalent length. In this methodology, resistance is calculated using a bulb-less ship with all the same properties of the ship with a bulb, except that the characteristic length (L_{bp} or L_{wl}) is increased to match the power requirements of the ship with a bulb. This length increase varies with Froude number. Per [23], for Froude numbers between 0.22 and 0.25, the ship's length is increased by about half of the length that the bulb projects forward of the forward perpendicular; for Froude numbers between 0.3 and 0.33, the ship's length should be increased by up to three times the length of the bulb. This methodology has a great deal of error inherent in it, mainly because the forms of bulbs vary greatly and it is difficult to capture the interaction of the bulb with the hullform using this rather coarse tool.

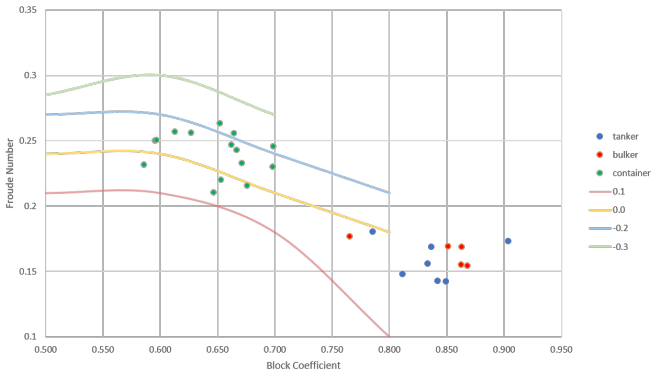

Fig. 52: Ship data for new ships with bulbs plotted alongside Guldhammer & Harvald coefficients of resistance.

b) Hollenbach: Hollenbach [1] addresses the bulbous bow by increasing ship length by the length of the bulb, similar to the method suggested by Schneekluth and Bertram, except the added length is not modified for various speeds. This method does not allow comparison of hullforms with and without a bulb, as the hullform without a bulb demonstrates higher resistance even at very low speeds where frictional resistance is dominant and thus where the bulb should increase ship resistance.

c) Kracht: Kracht [13] performed an in-depth study of the performance of various bulbous bow forms and the impact that several parameters have on the performance of the bulb. These parameters include length, width, height, volume, and position and shape of the bulb, all related to equivalent data of the bare ship hull. Kracht defines a residual power reduction coefficient, $\Delta C_{P\nabla R}$, to capture the change in residual resistance for a ship with and without a bulb,

$$\Delta C_{P\nabla R} = 1.0 - C_{Rwith}/C_{Rwithout}, \tag{23}$$

where C_{Rwith} and $C_{Rwithout}$ are residual resistance coefficients of equivalent ships with and without a bulb. Figure 53 shows the variation of $\Delta C_{P\nabla R}$ with Froude number for various bulb shapes and baseline hulls. All of these example ships have a block coefficient of approximately 0.7. Note the variation of impact of the bulb with Froude number, and thus

with speed of the ship.

Kracht produced a set of design curves that assist in the selection of the properties of a bulb for a given application. We find that using these curves to predict bulb size on modern cargo ships significantly under-predicts the size of the bulb that is actually installed on the ships we tested, possibly due to the amount of noise in the prediction charts, due to advances in bulb design, or due to changes in ship design and performance over the years.

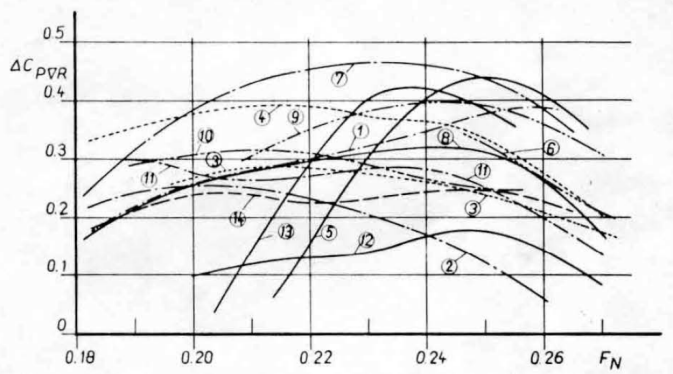

Fig. 53: Residual power reduction coefficient as a function of Froude number for various ship-bulb combinations [13]. All ships have a block coefficient very close to 0.7.

d) Kristensen and Lützen: Kristensen and Lützen [14] provide separate equations to estimate of the resistance impact of bulbous bows for container ships and for bulk carriers and tankers, derived from the examination of several model test results for ship hulls with bulbous bows, compared to equivalent bulb-less hull resistance calculated by Harvald's method. They argue that the impact of a bulbous bow depends primarily on three parameters: the length-displacement ratio, the prismatic coefficient, and the Froude number, Fr. They further argue that, for tankers, the length-displacement ratio and Froude number vary within a very tight range, so they present an equation for estimating resistance impact of a bulbous bow for a tanker as a function of Froude number only

$$\Delta C_{R,bulb} = max(-0.4, -0.1 - 1.6Fr). \quad (24)$$

This bulb correction is negative, thus reducing resistance, for all vessels at all speeds. For a container ship, the correlation is found to be

$$\Delta C_{R,bulb} = (250Fr - 90) \cdot \frac{C_{R,HarvaldNOBulbousBow}}{100}. \quad (25)$$

where $C_{R,HarvaldNOBulbousBow}$ is the coefficient of resistance for the equivalent ship without a bulbous bow calculated using the Harvald estimation process. This bulb correction is negative for expected Froude numbers.

The data upon which Kristensen and Lützen based their equations are shown in Figure 54 for equation (24) and Figure 55 for equation (25). One can see that there is significant noise in the data.

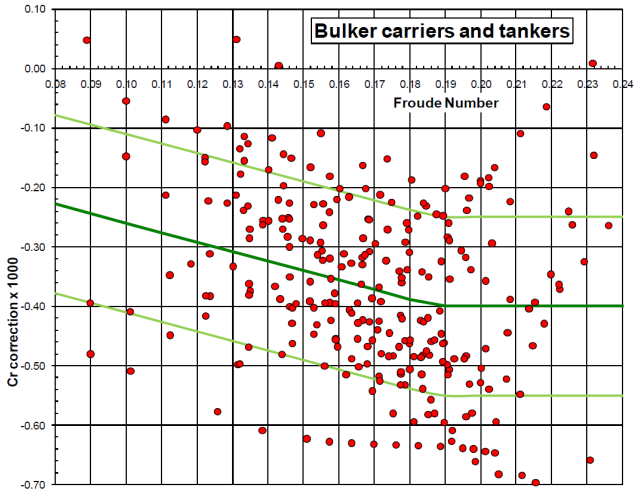

Fig. 54: Bulbous bow resistance correction plotted for 277 model tests of 16 tanker and bulk carrier vessels at various loading conditions and speeds, from [14].

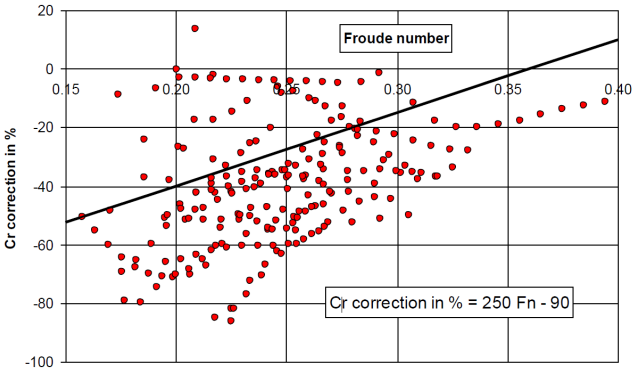

Fig. 55: Bulbous bow resistance correction plotted for 229 model tests of 21 different container, ro-ro and general cargo ships, all with block coefficients in the range of 0.5 - 0.7, from [14].

e) Holtrop and Mennen: Holtrop & Mennen multiply the wave resistance by a constant value, c_2, where $0 < c_2 \leq 1$, thus reducing the wave resistance by a constant percentage across the full range of ship speeds. The coefficient c_2 is a function of bulbous bow transverse cross-sectional area at the forward perpendicular, A_{bt}; height of the centroid of this area, h_b, compared to ship draft forward, T_f; and ship beam, B, and draft, T, as follows:

$$c_2 = e^{-1.89\sqrt{c_3}}$$

where

$$c_3 = \frac{0.56A_{bt}^{1.5}}{BT(0.31\sqrt{A_{bt}} + T_f - h_b)}.$$

Although the Holtrop & Mennen method does not fully

capture the change in effect of a bulbous bow with Froude number around design speed, the estimation is a reasonable approach because at low speeds, the wave resistance is very low, so the bulb impact is low; and the ship does not typically move at speeds significantly above the design speed, so the inaccuracies at very high speeds are not pertinent.

D. Bulbous Bow Conclusions

The conclusions we have drawn from our review of bulbous bow analysis and estimation criteria are as follows:

- It is clear that a properly designed bulbous bow can reduce ship resistance.
- The reduction in wave resistance due to the bulb peaks at a specific Froude number and drops off with speeds both higher and lower than the peak, as shown in Figure 53.
- This reduction in ship resistance occurs within a window of speeds centered around the speed for which the bulb is designed. Outside this window, the bulb has very little effect and can even have an adverse effect as shown in Figure 19.
- No simple estimation method exists that can accurately calculate the impact of the bulb on the ship's resistance, especially over a range of speeds and loading conditions. Bulb performance varies widely as shown in Figures 53, 54 and 55. This is because the bulb shape is designed in conjunction with the ship hull to tailor flow to a specific operational condition. Accurate estimation of the ship's resistance with a bulb requires model testing or CFD analysis of the ship's lines.
- Recommendations for a new bulb tailored to a new operating speed cannot be accomplished using standard-series-level or regression-analysis-level data; it requires either model testing or CFD.
- We find that Holtrop's method works as well as any of the methods available for estimating the impact of the bulbous bow on resistance, and better than many, and has the further recommendation that it is in keeping with the remainder of the Holtop resistance estimation method that we employ.
- We provide a ballpark-level estimate of savings found through removal of the bulb. If this appears advantageous, we recommend more detailed analysis prior to committing to any structural changes.

GLOSSARY

Δ	displacement at design condition	
Δ_B	displacement at ballast condition	
∇	volumetric displacement at design condition	Δ/ρ
∇_b	bulbous bow volumetric displacement	
ν	kinematic viscosity of sea water	$1.1945 \cdot 10^{-6}(m^2/s)$
ρ	density of sea water	1026 kg/m^3
ρ_a	density of air	1.225 kg/m^3
η_h	propeller hull efficiency	(1-w)/(1-t)
η_o	open water propeller efficiency	
η_r	propeller relative rotative efficiency	
η_s	shaft efficiency	
σ	local cavitation number	
τ_c	cavitation thrust coefficient	
A_b	surface area of the bulbous bow	
A_{bt}	transverse cross-sectional area of the bulbous bow at the forward perpendicular	
A_E	propeller expanded area	
A_{exp}	the transverse cross-sectional area of the hullform and cargo above the waterline	
A_P	propeller projected blade area	
A_{wp}	waterplane area	
A_{ws}	wetted surface area of the hull	
A_{wsB}	wetted surface area of the hull at ballast	
A_x	transverse area of midship section below waterline	
AE/AO	propeller expanded area ratio	
B	beam at waterline	
C_a	correlation allowance	
C_{aa}	air resistance coefficient	0.8
C_{app}	coefficient of frictional resistance for appendages	
C_b	block coefficient	$\Delta/(L_{wl}BT)$
C_f	coefficient of frictional resistance	
C_p	prismatic coefficient	$(A_x L_{wl})/(L_{wl}BT) = C_b/C_x$
C_r	coefficient of residual resistance	
C_{stern}	Holtrop stern shape parameter	
C_{th}	thrust coefficient	
C_v	viscous resistance coefficient	
C_{wp}	waterplane area coefficient	$A_{wp}/(L_{wl}B)$
C_x	midship section coefficient	$A_x/(BT)$
CSR	engine continuous service rating	
D	propeller diameter	
d_{ap}	distance between aft perpendicular and aftmost point of the wet hull	
ECT	diesel engine electronic control tuning	
EGB	exhaust gas bypass, a diesel engine tuning methodology	
em	engine margin	
F_{trim}	trim factor	
Fr	Froude number	$Fr = U/\sqrt{gL}$
Fr_c	critical Froude number	
FOC	fuel oil consumption	
g	gravitational constant	9.81 m/s^2
h	depth of center of propeller hub below water surface	
h_b	height of the centroid of A_{bt} above the baseline	
h_z	height of the center of the propeller hub above the baseline	
i_e	entrance half-angle	
J	propeller advance ratio	V_a/nD
K_Q	propeller torque coefficient	
K_T	propeller thrust coefficient	
L_b	length of bulbous bow extending forward of forward perpendicular	
L_{bp}	ship length between perpendiculars	

L_c	Hollenbach characteristic length	
L_{oa}	ship length overall	
L_{os}	overall length of wetted surface	
L_r	Holtrop & Mennen length of run of ship	
L_{wl}	ship waterline length	
lcb	longitudinal center of buoyancy with respect to $\frac{1}{2}L_{wl}$ as percent of L_{wl}, positive forward	
lcb_{ap}	longitudinal center of buoyancy of the ship measured from the aft perpendicular	
lcb_b	longitudinal center of buoyancy of the bulbous bow	
MCR	engine maximum continuous rating	
MEP	engine mean effective pressure	
N	engine rotation rate	
N_{SMCR}	engine rotation rate at SMCR	
N_p	number of propellers	
n	rotation rate of propeller	
P_b	brake power	P_d / η_s
P_d	delivered power	$P_e/\eta_o\eta_h\eta_r$
P_e	effective power	
Pb_{SMCR}	engine brake power at SMCR	
P/D	propeller pitch-to-diameter ratio at 70% of the radius	
p_{atm}	atmospheric pressure	101,300 Pa
p_v	vapor pressure of seawater	2,291 Pa at 20^oC
p_0	hydrostatic pressure	$p_0 = p_{atm} + \rho gh$
pm	propeller margin	
Q_o	open water torque	
R_a	correlation allowance resistance adjustment	
R_{aa}	air resistance	
R_{app}	total frictional resistance of all appendages	
R_f	frictional resistance	
R_r	residuary resistance	
R_T	total resistance	
R_{TC}	total resistance at trial condition	
R_{HR}	total resistance at heavy running condition	
R_w	wave resistance	
Re	Reynold's number	VL/ν
S_{app}	appendage surface area	
SFOC	specific fuel oil consumption	
SMCR	engine specified maximum continuous rating	
T	mean draft at design condition	$(T_a + T_f)/2$
T_a	draft at the aft perpendicular at design condition	
T_f	draft at the forward perpendicular at design condition	
T_B	mean draft at ballast condition	
T_{aB}	draft at the aft perpendicular at ballast condition	
T_{fB}	draft at the forward perpendicular at ballast condition	
Th	thrust	$R_T/(1-t)$
T_o	open water thrust	
TCCO	turbocharger cut-out, a diesel engine tuning methodology	
t	thrust deduction factor	
t_B	thrust deduction factor at ballast condition	
V	ship speed	
V_a	water speed at the propeller	$V(1-w)$
V_R	relative velocity of water at 0.7 of the propeller radius	
VTA	variable turbine area, a diesel engine tuning methodology	
w	wake fraction	
w_B	wake fraction at ballast condition	
Z	number of propeller blades	
$(1+k)$	frictional form factor	
$(1+k_2)$	appendage resistance factor	

MIT SEA GRANT COLLEGE PROGRAM

MIT SEA GRANT REPORT NUMBER
2019-R/RCM-64-LEV
9/23/2021

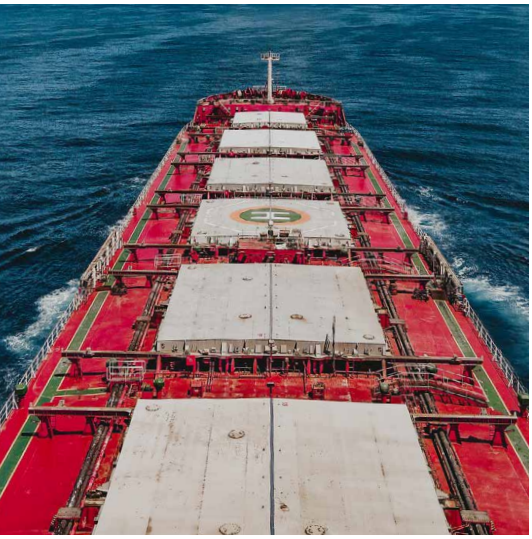

Propeller curves for a representative propeller

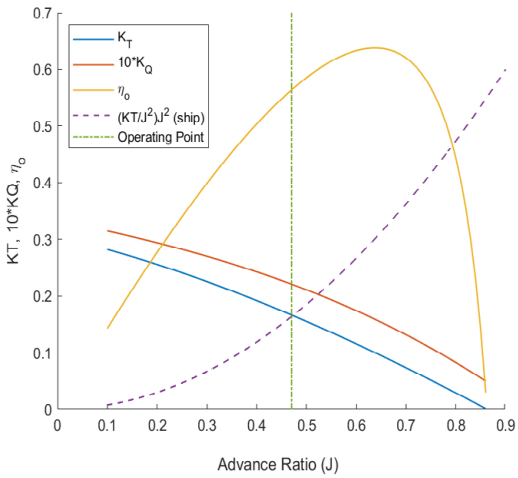

Representative engine load and operating limits for an engine installed in a ship